

UNIVERSITY OF CINCINNATI

DATE: August 16, 2002

I, Gregory J. Stelzer,
**hereby submit this as part of the requirements for the
degree of:**

Master of Science

in:

Mechanical Engineering

It is entitled:

A Magnetorheologic Semi-Active Isolator To Reduce Noise And
Vibration Transmissibility In Automobiles

Approved by:

Dr. Mark J. Schulz

Dr. Jay Kim

Dr. Randall J. Allemang

A MAGNETORHEOLOGIC SEMI-ACTIVE ISOLATOR TO REDUCE NOISE AND VIBRATION TRANSMISSIBILITY IN AUTOMOBILES

A thesis submitted to the

Division of Research and Advanced Studies
of the University of Cincinnati

In partial fulfillment of the
requirements for the degree of

MASTER OF SCIENCE (MS)

in the Department of Mechanical, Industrial and Nuclear Engineering
of the College of Engineering

2002

by

Gregory J. Stelzer

B.S.M.E., University of Cincinnati, 2000

Co-Advisors: Dr. Mark J. Schulz
 Dr. Jay Kim
Committee Member: Dr. Randall J. Allemang

Abstract

The automotive industry is increasingly competitive, and manufacturers are seeking even small advantages for their product through innovative designs, lower cost parts, and more efficient manufacturing. Low cost is important, and initiatives by the automobile manufacturer to reduce cost cascade down to the different tiers of suppliers. In this process, durability of components is often considered before noise and vibration harshness, especially on low-end vehicles. Also, noise control expectations from the end user are recently becoming more demanding.

Automotive manufacturers have responded by placing further expectations on the suppliers, and stringent noise control specifications are now standard on many of the smallest components in the vehicle. The demand for cost reduction, noise reduction, and increased operator comfort together requires that new approaches be developed for noise and vibration isolation in automobiles.

The objective of this thesis is to develop a new isolator design for automotive components that can provide substantial and cost-effective improvements in noise and vibration harshness performance. To achieve this goal, passive, semi-active, and active isolator designs and different types of smart materials were investigated. Based on this study, the most promising approach turned out to be a semi-active magnetorheologic isolator. This type of isolator was modeled and optimized to reduce noise transmission while maintaining durability performance for an automotive component. The new results that this study produced are: (i) a detailed nonlinear model of a magnetorheologic isolator and semi-active control system, (ii) detailed simulation studies showing the trade-offs between passive and semi-active isolator performance for automotive components, and (iii) a new isolator design that provides durability and isolation performance that cannot be achieved using a passive isolator alone. The isolator

design is based on a compressor component mounted to the frame of an automobile, but the isolation technique also has other applications. These include engine mounts, suspensions, and pumps in automobiles, and applications where the isolator must be durable to withstand low frequency vibration and shock loading, and at the same time prevent transmissibility of high frequency vibration from the component to the mounting structure that causes noise inside the automobile.

Acknowledgements

I would like to acknowledge three groups of people who have supported me through my research. First, I would like to thank the faculty at the University of Cincinnati, in particular Dr. Mark J. Schulz. With his help and flexibility, I have been able to do most of my work from my home in Dayton. This allowed me to work a full time job, and achieve my master's degree. I would also like to thank Dr. Jay Kim and Dr. Randall J. Allemang for being committee members.

Second, I would like to thank my co-workers at Delphi Automotive Systems. I would like to thank my supervisors, Mike Riehle and Brent Dunlap, for allowing me the flexibility to do what I needed to do to finish both my work and school obligations. I would also like to acknowledge the following, in alphabetical order, for their help, Matt Cukovecki , Patrick Hopkins, Chad Michael, Jamshid Moradmand, Wit Nursilo, and Sanjiv Tewani.

Finally, I would like to thank my family and friends for their support throughout the various stages of my master's program. Their calming words and well-timed humor have allowed me to keep my sanity through this process.

Table of Contents

LIST OF TABLES	4
LIST OF FIGURES	4
LIST OF SYMBOLS	6
CHAPTER 1 – INTRODUCTION	
1-1. General	7
1-2. Structure of the Thesis	9
CHAPTER 2 – METHODS OF VIBRATION ISOLATION	
2-1. Passive Isolation Systems	11
2-2. Semi-Active Isolation Systems	18
2-3. Active Isolation Systems	18
2-4. Smart Materials for Actuators	19
CHAPTER 3 – MODELING OF RHEOLOGIC FLUIDS	
3-1. ER/MR Fluid Isolator Systems	21
3-2. Bingham Plastic Model of the MR Fluid	22
3-3. MR Working Modes	24
CHAPTER 4 – MODELING THE ISOLATION SYSTEM	
4-1. Simulation of the Passive Isolator	27
4-2. Simulation of the Semi-Active Isolator	31
4-3. System Inputs	36
4-4. System Outputs	37
4-5. Newmark-Beta Explicit Time Integration Method.....	38
4-6. Filter Design	38
4-7. Control Law Design	43

4-8	Detailed Design of the MR Isolator	48
CHAPTER 5 – ISOLATION SIMULATION STUDIES		
5-1.	Results for the Passive Isolation System	50
5-2.	Results for the Semi-Active Isolation System	52
CHAPTER 6 – MR ISOLATOR COIL DESIGN		
6-1.	Determining Necessary Yield Stress	60
6-2.	Electromagnetic Model of the Isolator	61
6-3.	Coil Properties	63
6-4.	Final Design	67
CHAPTER 7 – CONCLUSIONS		
7-1.	Comments	71
CHAPTER 8 – RECOMMENDATIONS FOR FUTURE WORK		
8-1	Items for Future Research	73
BIBLIOGRAPHY		75
APPENDIX A		79
• Computer Algorithm to Compute Transmissibility of a Passive Isolator		
APPENDIX B		81
• Computer Algorithm for the Single Degree of Freedom Passive Model		
APPENDIX C		85
• Computer Algorithm for the Single Degree of Freedom Semi-Active Model		
APPENDIX D		92
• Coil Design Equations		
APPENDIX E		94

- Algorithms for: (1) compressor input, (2) vehicle body input, (3) low pass filtering, and (4) skyhook and relative skyhook control

LIST OF TABLES

5.1	Summary of simulation results	56
6.1.	Final design parameters	68
6.2.	Mass of the semi-active isolator	70

LIST OF FIGURES

1.1	A compressor assembly with passive isolators	9
2.1	Design of a passive isolator	12
2.2	Design of a passive hydromount	13
2.3	Transmissibility model	14
2.4	Transmissibility as a function of stiffness	16
2.5	Transmissibility as a function of damping	17
3.1	Shear stress versus shear strain rate for a Bingham plastic material	23
3.2	Viscosity is a function of shear rate	23
3.3	Yield stress as a function of magnetic field	24
3.4	Working of MR fluid in shear mode	25
3.5	Working of MR fluid in flow mode	25
3.6	Working of MR fluid in squeeze mode	26
4.1	Passive model	28
4.2	Passive free body diagram	29
4.3	Semi-active model	32
4.4	Semi-active free body diagram	33
4.5	Model input for the compressor and vehicle body	36
4.6	Example of power spectral density plot	37
4.7	Characteristics of a second order Butterworth filter	39

4.8	Showing the phase lag with a Butterworth low-pass filter	40
4.9	Characteristics of an ideal low-pass filter	41
4.10	Reaction of isolator components with filter off	43
4.11	Diagram of skyhook control law	45
4.12	Skyhook control does not allow the isolator to react properly	46
4.13	Diagram of relative skyhook control law	46
4.14	No skyhook control allows the isolator to react properly	47
5.1	Effect of passive stiffness on transmitted force	50
5.2	Effect of passive stiffness on maximum relative displacement	51
5.3	Transmitted force results from the semi-active system	53
5.4	Maximum relative displacement results from the semi-active system ...	54
5.5	Improvement to relative displacement with MR fluid	55
5.6	Relative displacement and isolator component with filter off	58
5.7	Viscosity is dependant on relative velocity	59
6.1	Yield stress and magnetic flux in model	60
6.2	Coil design with intended flux pattern	61
6.3	Finite element results showing flux in the isolator	62
6.4	Number of coils and coil mass as a function of wire gage	64
6.5	Coil length and resistance as a function of wire gage	65
6.6	Voltage and current needed to achieve 500 amp turns	66
6.7	Proposed design of a MR base semi-active isolator	67
6.8	Power requirements of the semi-active isolator	69

LIST OF SYMBOLS

f_{yield}	active MR component	τ_{MR}	yield strength of MR fluid
τ_y	yield strength of MR fluid	τ_o	yield strength of MR fluid
c_{MR}	passive MR component	η	MR fluid viscosity
x	compressor displacement	y	vehicle body displacement
\dot{x}	compressor velocity	\dot{y}	vehicle body velocity
$\dot{\gamma}$	shear rate	F_i	force
H	magnetic induction	v	velocity
B	magnetic flux	p_i	pressure
f	MR force	b	width of flow channel
S	flow cross sectional are	h	height
L	length of flow channel	Q	fluid flow rate
k	passive stiffness	c	passive damping
zeta	damping coefficient	A_i	Area of inner diameter of isolator
A_o	area of outer diameter of isolator	a	radius of electrode
A_{gap}	Area of gap between inner and outer diameter		
r_o	outer radius	r_i	inner radius
ω	frequency of compressor	ω_n	natural frequency of isolator
h	original height of plunger	$h(t)$	height of plunger at time t
ΔP	total change in pressure	$\Delta P_{0,HF}$	change in pressure from viscosity
$\Delta P_{ER,HF}$	pressure change from yield stress	$\Phi(x)$	non-dimensional output force

CHAPTER 1. INTRODUCTION

1.1 General

With increasing competition, the automotive industry is implementing improvements through innovative designs, lower cost parts, and more efficient manufacturing methods. Cost reduction is important to increase competitiveness, and cost reduction efforts by the manufacturers cascade down to the different tiers of suppliers. In regard to cost reduction of components, durability issues are often more important than Noise and Vibration Harshness (NVH), especially on low-end vehicles. At the same time, noise control expectations from the end user are becoming more demanding. A customer will now use component performance and cost to develop a list of acceptable candidates, and then use NVH to determine where the business is awarded. This has prompted the automotive manufacturers to respond by placing still higher expectations on the suppliers, and stringent noise control specifications are now standard on many of the smallest components in the vehicle. The demand for cost reduction, noise reduction, and increased operator comfort together is requiring that improved or new approaches for vibration and noise isolation and attenuation in automobiles be developed.

Most vibration isolation systems in automobiles are passive systems. This is the cheapest and simplest option. However, there is a tradeoff between cost and NVH performance. This tradeoff hinges on the issue of durability (i.e. passive isolators cannot provide both optimal isolation and satisfactory durability). The object of this thesis is to develop an advanced isolator design for automotive components that can provide substantial and cost-effective improvements in NVH performance. To achieve this goal, passive, semi-active, and active isolator designs and different types of smart materials were investigated. The investigation involved surveying

existing approaches for vibration isolation and current practice for isolator design in the automobile industry. Based on the isolator design study, the most promising approach was determined. This design reduced noise transmission while maintaining durability performance.

The component considered in this thesis that produces the high frequency excitation and that will be mounted using the isolator will be assumed to be a compressor, and will be referred to as such throughout the rest of the thesis. A picture of a compressor and its passive isolators can be seen in Figure 1.1. Specifically, the goal of the thesis is to design a soft isolator to isolate the vibration of the compressor from the vehicle body to prevent noise inside the automobile. The isolator must also withstand the loading due to low frequency vibration and shock, and maintain an acceptable displacement relative to the automobile body. The low frequency vibration of the automobile and suspension occurs during normal operation of the vehicle, and the shock input occurs when the vehicle hits a bump. Passive isolators are not optimal for these design requirements. A soft passive mount will isolate the high frequency vibration produced by the compressor to prevent noise inside the automobile, but the mount will not meet the durability or displacement requirements at low frequency. A stiff passive mount will meet the durability and displacement requirements at low frequency, but it will not isolate the automobile body from the high frequency vibration produced by the compressor.

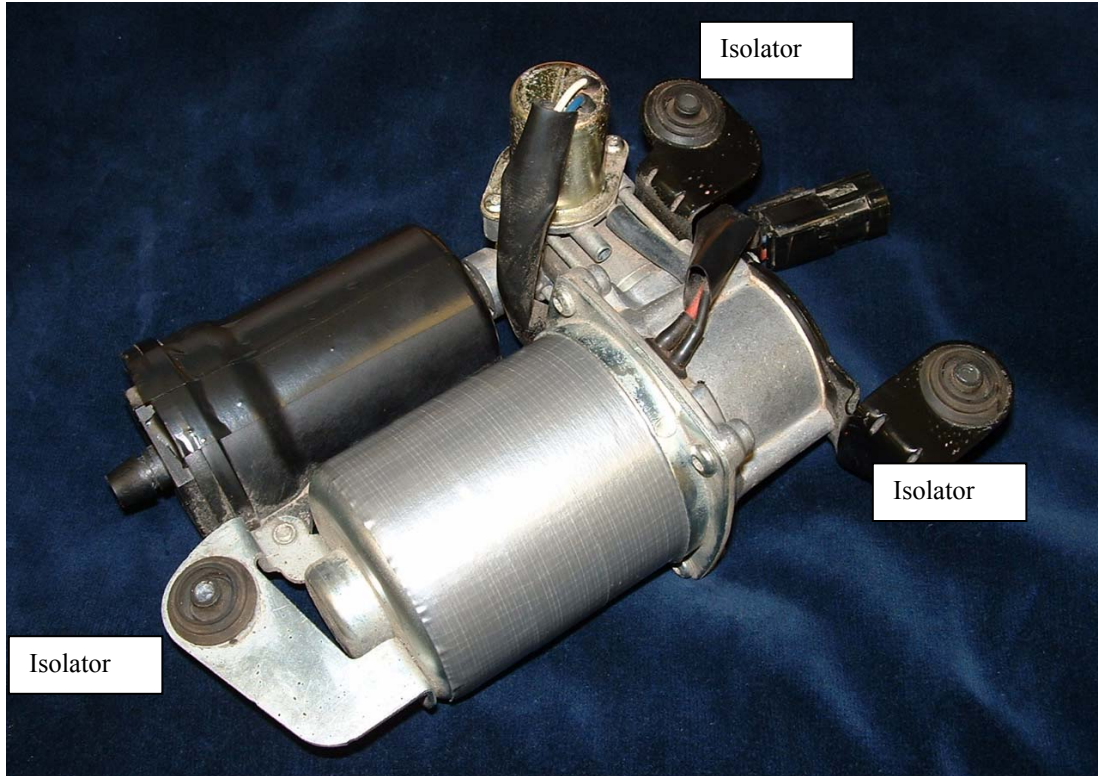


Figure 1.1. A compressor assembly with three passive rubber isolators.

1.2 Structure of the Thesis

This thesis contains eight chapters and is organized in the following way. Chapter 2 discusses the principle of vibration isolation and shows different types of isolation systems. Passive, semi-active, and active isolation systems are discussed, and the differences between the systems are brought out. Also, the use of smart materials for actuators, including piezoelectric ceramics, Shape Memory Alloy (SMA) wires, and rheologic fluids are discussed. In Chapter 3, the use of Electro-Rheologic (ER) and Magneto-Rheologic (MR) fluid dampers in semi-active systems is explored. The discussion looks at the earliest research projects involving these fluids and the strengths and weaknesses of each fluid damper. Finally, the different working modes of MR

fluids are discussed. Chapter 4 introduces the models used for the passive and semi-active systems. A derivation of equations for each model is shown. Filter designs and control laws for the semi-active system are presented and advantages of each design are discussed. The Newmark-Beta explicit time integration method with a force balance iteration used in each model is explained. The important inputs and outputs of the model are discussed. The chapter ends by looking at a detailed design of the MR isolator. Chapter 5 characterizes the system performance using simulation results from the passive and semi-active systems. Chapter 6 discusses the coil design issues. Parameters required to design an adequate coil to provide the necessary magnetic field are discussed. Chapter 7 gives conclusions of the thesis. Recommendations for further work are given in Chapter 8.

CHAPTER 2. METHODS OF VIBRATION ISOLATION

A vibration isolator is a flexible device that is used to attach a component to a mounting base. The purpose of the isolator is to reduce the vibration or force transmitted between the component and the base. In this chapter, different possible approaches for vibration isolation of automobile components are described and compared, and the optimal approach for a particular automotive application is determined.

2.1 Passive Isolation Systems

Based on cost, many isolation systems use passive components. In this case, no controls are needed for the isolator. With a passive system, it is easy to design for durability specifications. A couple designs are common and will be discussed.

Often the design consists of a simple natural rubber material, or a comparable synthetic material with attachments. This is the cheapest option, in that it is the simplest design and easiest to manufacture. If a particular compressor/isolator is a durability risk, the isolation can be stiffened by simply changing the material or increasing the durometer hardness value for the rubber material, or increasing the size of the isolator. If high temperatures affect the performance of the isolators, the durometer can be increased or a material less susceptible to temperature can be chosen. However, as the stiffness of the isolators is increased, the noise performance of the compressor will be compromised because a stiffer mount will generally transmit higher frequency vibration [1].

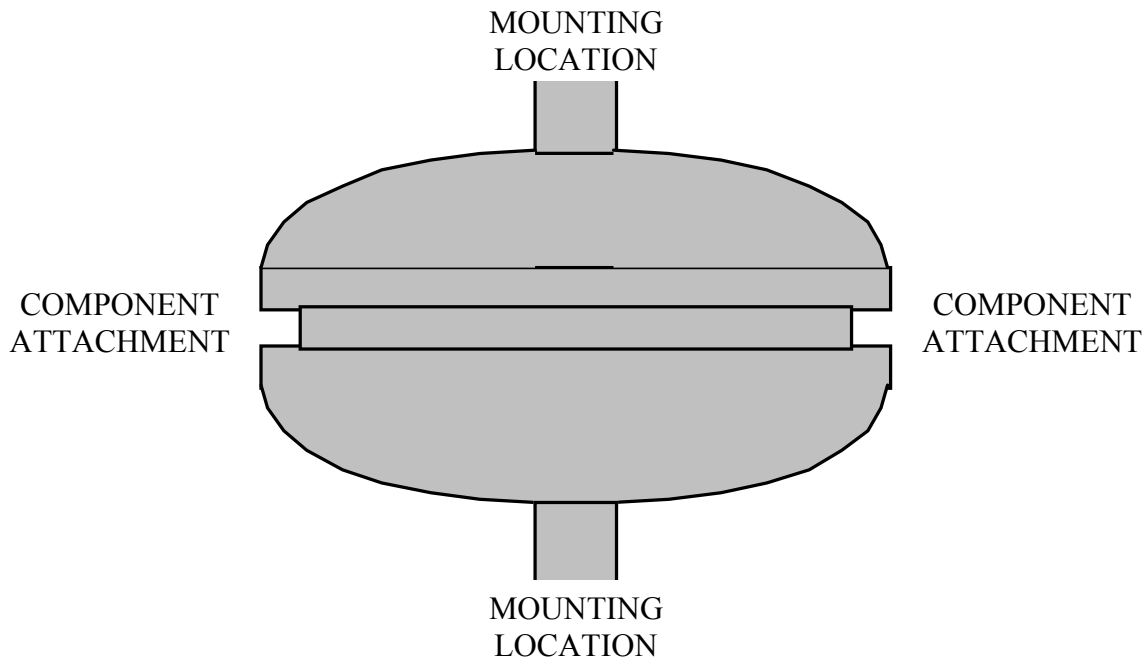


Figure 2.1. Design of a passive isolator.

The hydromount is another passive isolator. Here, fluid is incorporated into the design. The fluid is forced through an orifice within the isolator. The resistance provided by the orifice provides damping for the isolated component, a compressor in this case, allowing the isolator to be made of a less stiff material. The combination of reduced stiffness and increased damping allows the hydromount to provide better isolation without compromising durability. However, the added damping increases the transmitted force, and therefore, the system can never be optimized [1].

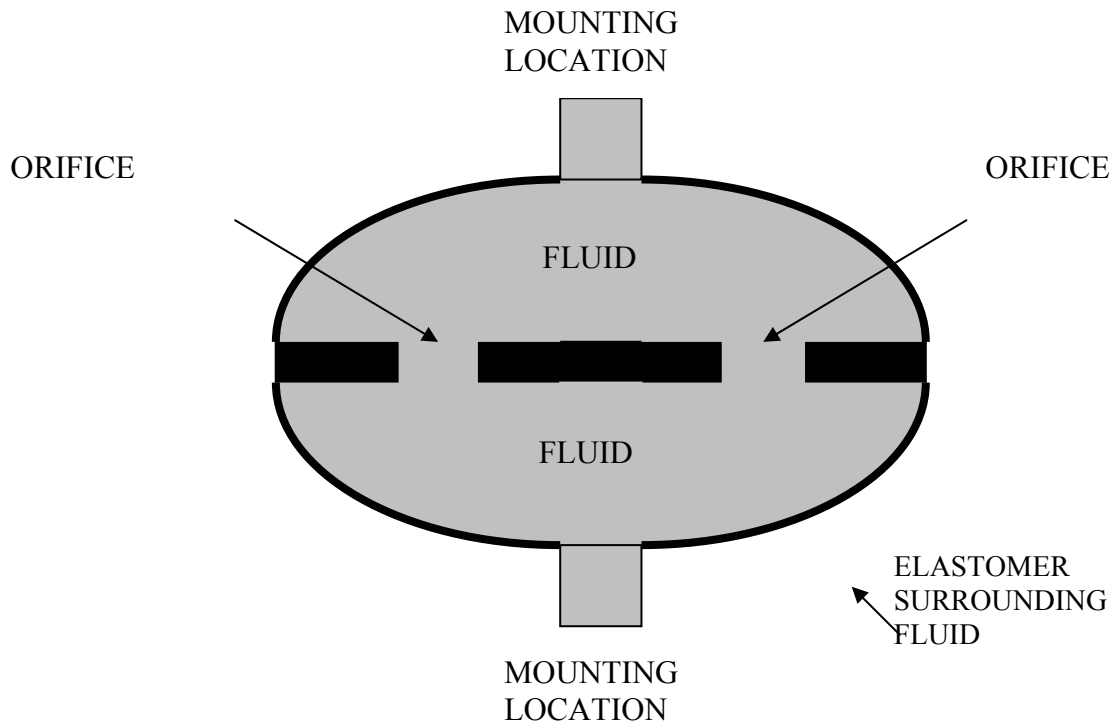


Figure 2.2. Design of a passive hydromount.

The transmissibility model can be seen in Figure 2.3. The model shows a component mounted to a base through an isolator that has only passive stiffness and passive damping components (k and c , respectively) [2].

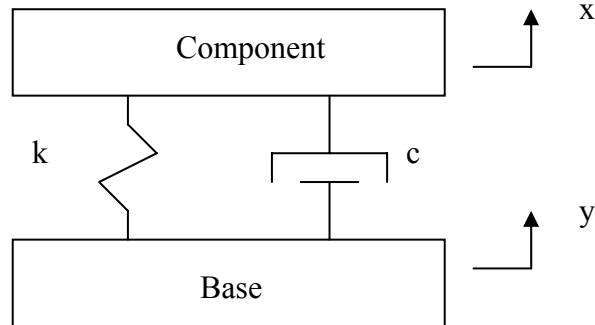


Figure 2.3. Transmissibility Model.

The transmissibility model is used to create a ratio between force seen in the components due to rotating unbalance and force transmitted through the isolator into the base. This ratio is dependent upon frequency and the mass, damping, and stiffness characteristics of the system. The ratio is developed by summing the forces seen in the model. This is seen in Equation (2.1).

$$\sum F + \uparrow = m\ddot{x} = k(y - x) + c(\dot{y} - \dot{x}) \quad (2.1)$$

Making the assumption that $x = Xe^{j\omega t}$ and $y = Ye^{j\omega t}$, where the real part is the displacement for the component and base, respectively. Velocity and acceleration can be calculated by taking the derivative of the displacement.

$$x = Xe^{j\omega t} \quad (2.2)$$

$$y = Ye^{j\omega t} \quad (2.5)$$

$$\dot{x} = j\omega Xe^{j\omega t} \quad (2.3)$$

$$\dot{y} = j\omega Ye^{j\omega t} \quad (2.6)$$

$$\ddot{x} = -\omega^2 Xe^{j\omega t} \quad (2.4)$$

$$\ddot{y} = -\omega^2 Ye^{j\omega t} \quad (2.7)$$

Incorporating these equations gives:

$$m\omega^2 X e^{j\omega t} = k(Y e^{j\omega t} - X e^{j\omega t}) + c(j\omega Y e^{j\omega t} - j\omega X e^{j\omega t}) \quad (2.8)$$

The $e^{j\omega t}$ component cancels:

$$-m\omega^2 X = kY - kX + j\omega cY - j\omega cX \quad (2.9)$$

where X and Y are the amplitudes of vibration and ω is the speed of the component. Equation (2.9) is rewritten as:

$$[k - m\omega^2 + j\omega c]X = [k + j\omega c]Y \quad (2.10)$$

Solving, the amplitude of the mass, X , divided by the amplitude of the base, Y , gives the transmissibility:

$$\frac{X}{Y} = \frac{k + j\omega c}{k - m\omega^2 + j\omega c} \quad (2.11)$$

Using Equation 2.4, transmissibility curves for passive systems can be seen in Figure 2.4 and 2.5. Figure 2.4 shows the change in transmissibility as stiffness is changed.

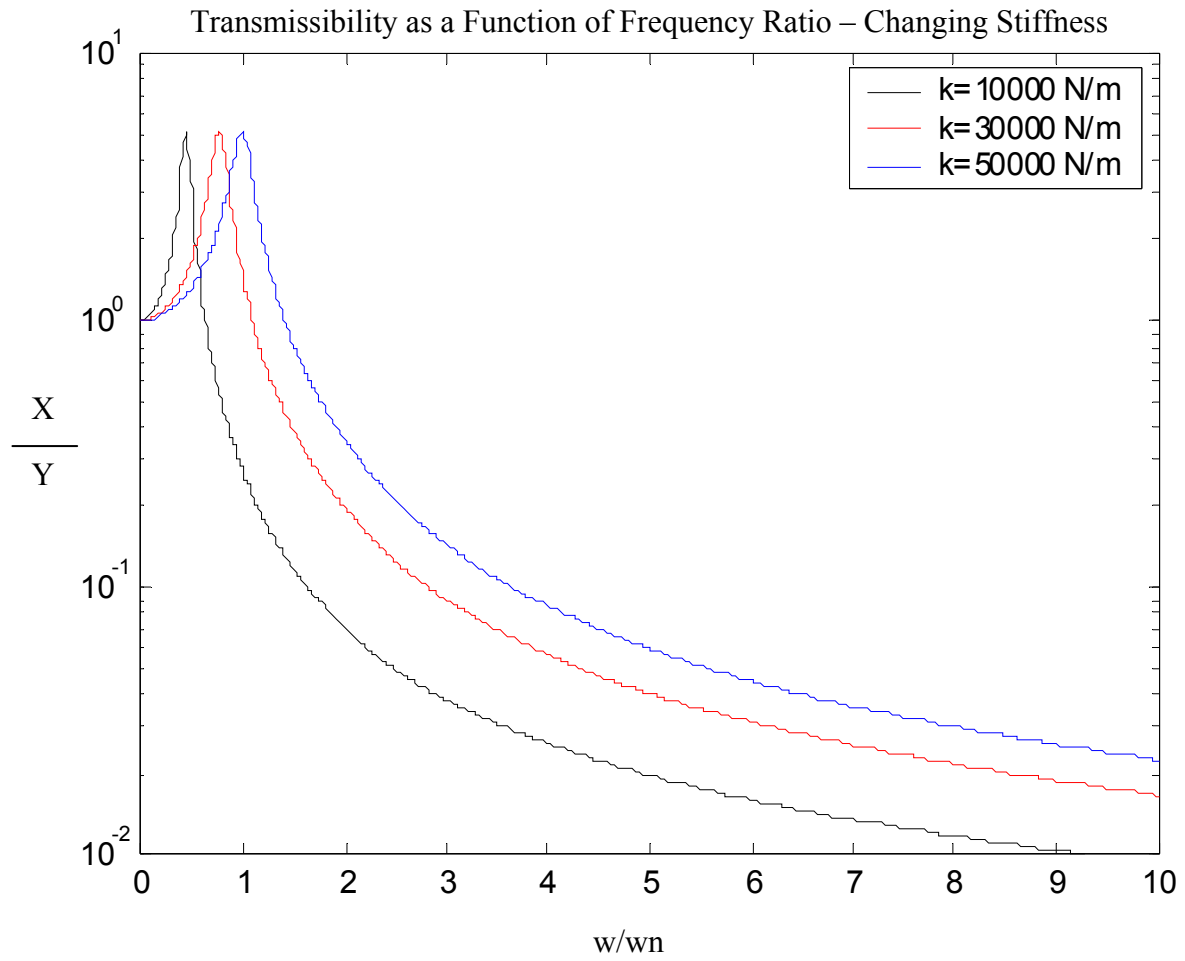


Figure 2.4. Transmissibility as a function of the stiffness of the isolator.

Figure 2.5 shows the effect on transmissibility as damping is changed. The algorithm developed to perform the transmissibility simulation is listed in Appendix A.

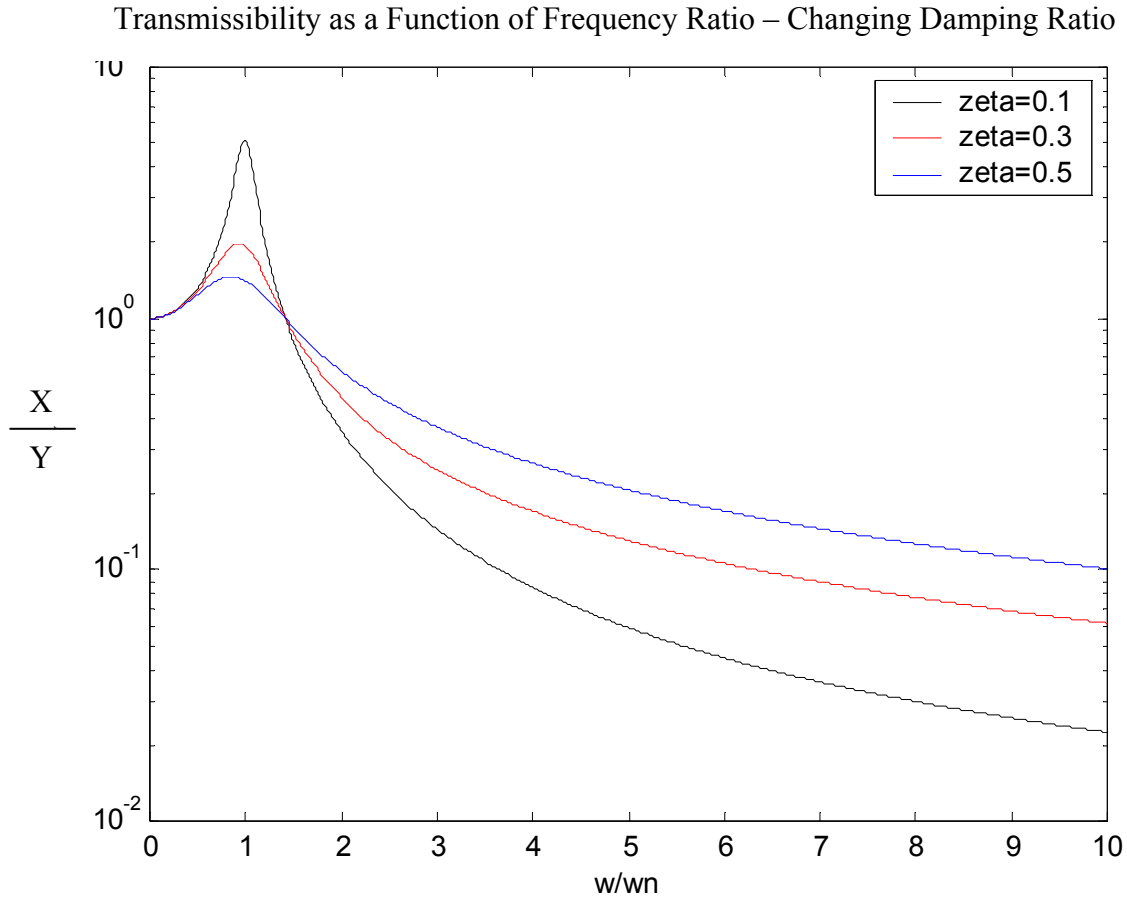


Figure 2.5. Transmissibility as a function of the damping of the isolator.

These figures show that transmissibility increases as stiffness and damping increase, assuming the frequency of concern is well above the natural frequency of the isolator. It is understood that these designs are inexpensive, and it will be shown that the passive isolator can be effective in addressing durability issues. However, the two figures show that noise transmission will be adversely affected if stiffness or damping are increased to address durability.

An inflection point is seen in Figure 2.5. At frequencies below the inflection point, transmissibility is above one, but damping reduces transmissibility. At frequencies above the inflection point, transmissibility is below one, but damping increases transmissibility. The point is located at roughly 1.4 times the natural frequency of the isolator, i.e. $\frac{\omega}{\omega_n} = 1.4$. This is why it is important to design a passive isolator to have a natural frequency significantly below the operating speed of the component.

2.2 Semi-Active Isolation Systems

A semi-active isolator is similar to a passive isolator, in that it can only remove energy from the system. However, a semi-active system is capable of changing one or more properties in response to a command signal [3]. In contrast, in a passive system properties are fixed. By having the capability to change system properties, a large amount of control can be gained with very little energy input. An example of a semi-active system is a shock absorber with a variable orifice that allows the damping coefficient to be changed as needed [3].

2.3 Active Isolation Systems

Active isolation systems can be controlled by computers through input signals from sensors. Unlike passive and semi-active systems, active systems are able to add energy to the system. An example of an active system is an electromechanical actuator arranged to generate force by responding to a velocity or displacement feedback signal.

The goal of active isolation is to provide energy equal in magnitude and opposite in phase to the vibration input. In doing so, an active isolation system can improve noise performance and durability performance. However, there is a serious drawback to the active system.

Active systems are very design intensive and require sensors and processors to provide real time data to the isolator. Large amounts of power are also required to operate an active isolator. These necessary features of the active isolation system make it the most expensive isolation design. For this reason, active isolation systems are very uncommon.

2.4 Smart Materials for Vibration Isolation

Several different materials that have been developed allow designers to use them as actuators in a system. Two examples of these materials are piezoelectric materials and shape memory alloys. Rheologic fluids can also be considered smart materials because they change properties based on an electric or magnetic field.

Piezoelectric materials experience a dimensional change when an electrical voltage is applied to them. Conversely, these materials produce an electrical charge when a pressure is applied to them [3]. The best known such material is lead-zirconate-titanate (PZT). The material can be bonded to a system or structure. If voltage coming from the material is monitored, it is operating as a sensor. If voltage is being supplied to the material in response to a feedback, the material is being operated as an actuator. The use of PZT for vibration isolation is limited due to the small strain capability of the material. A displacement amplifier would be needed when using PZT's for vibration isolation, and this increases the size, weight, and flexibility of the overall isolation system.

A shape memory alloy (SMA) material possesses the interesting property in that a metal “remembers” its original shape and size and changes back to that shape and size at a characteristic transformation temperature [3]. These properties have been found in gold-cadmium, brass, and nickel-titanium. The alloys inherent properties have become very useful to the medical field. Also, the SMA's ability to generate high forces at low frequencies allows the

material to be used as an actuator. However, the use of SMA in engineering applications has been limited due to the limited temperature range in which it can be effective and because of the slow response time.

Electro-Rheologic (ER) and Magneto-Rheologic (MR) fluids have the ability to change their yield strengths. Because of this, researchers have tried to incorporate the two materials in semi-active designs. While ER fluid reacts to an electric field and MR fluid reacts to a magnetic field, the two fluids operate in similar way. Tiny metal fibers are suspended in the fluid, and when a field is applied to the fluid, the metal fibers form strands in line with the field path.

These materials are particularly useful in vibration isolation systems. The vibration causes the strands of metal fibers to continually break. However, the field causes them to reform. It is this continual breaking and reforming of the strands of metal fibers that allows the fluid to dissipate energy from the system [1, 3, 4, 5].

CHAPTER 3. MODELING OF RHEOLOGIC FLUIDS

This chapter investigates fluids that change properties based on external fields. These fluids can be controlled to dissipate energy. The control used is semi-active, and with this approach minimal control energy can produce large actuation forces.

3.1 ER/MR Fluid Isolator Systems

A great deal of research has been conducted on semi-active systems to look for a compromise between passive and active isolation systems [1, 4]. The semi-active system has the ability to react to input from sensors providing real time control. However, it can only remove energy from the system. This approach can be used for vibration suppression or isolation and requires minimal power as compared to an active system. With a semi-active system, noise performance (reducing noise transmission) can be improved without dramatically hindering durability capabilities.

Extensive studies have been conducted on Electro-Rheologic (ER) and Magneto-Rheologic (MR) fluids for use in semi-active systems that are used for vibration suppression. Vibration suppression refers to reducing the vibration of a system with respect to a fixed base. The two materials were discovered in the late 1940's. Jack Rabinow [4, 5] reported on a MR fluid experimental program at the U.S. National Bureau of Standards for the Army's Chief of Ordinance in 1948 and Winslow publishing his account of a lengthy research program investigating the properties and applications of ER fluid in 1949. Both reports provided remarkable insight into the physical phenomena and anticipated present-day applications for the fluids.

Initial testing with ER fluids showed problems with the fluid, namely operating temperature limitations and storage stability problems. Over time, improvements have been made in these areas. However, new problems have arisen.

Today, ER fluids are considered to have low shear strengths. The fluid provides shear strengths that are two to ten times lower than needed for many practical applications. Also, high voltages are required to operate ER fluids, and there is a lack of a universal fluid. Because of these and other limitations, commercial success has been elusive.

MR fluids, on the other hand, have become more practical. When compared to ER fluids, MR fluids offer higher order yield stresses and provide a better operating temperature range. At the same time, companies such as Lord Corporation have commercial MR products. Because of the advantages of MR fluid over ER fluid, only MR fluid will be considered from this point.

3.2 Bingham Plastic Model of MR Fluids

MR fluid is traditionally modeled as a Bingham plastic, where there is a passive and active component to the fluid [3, 6]. The equation used to model the fluid is:

$$F_{MR} = f_{yield} + c_{MR}(\dot{x} - \dot{y}) \Leftrightarrow \tau_{MR} = \tau_y + \eta\dot{\gamma} \quad (3.1)$$

The passive component is a function of the fluid resistance from the viscosity, which is a property of the fluid and cannot be controlled. The active component is derived from the yield stress of the MR fluid, which changes proportionally with the applied magnetic field. The applied magnetic field can be controlled.

Initial research showed this resistance could be modeled as a constant, as seen in Figure 3.1

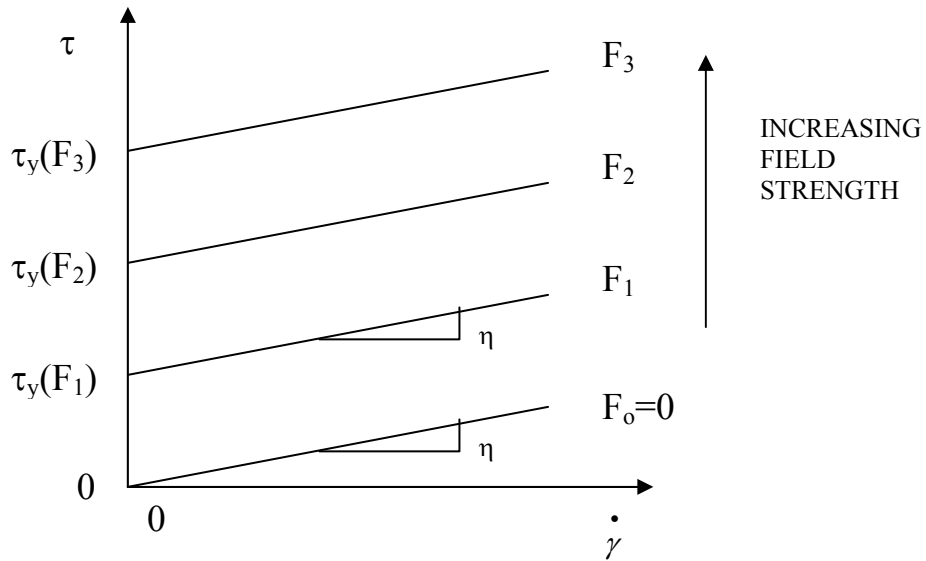


Figure 3.1. Shear stress versus shear strain rate for a Bingham plastic material.

However, further investigation showed that viscosity is a function of shear rate, with the viscosity increasing dramatically at lower shear rates. This is seen in Figure 3.2.

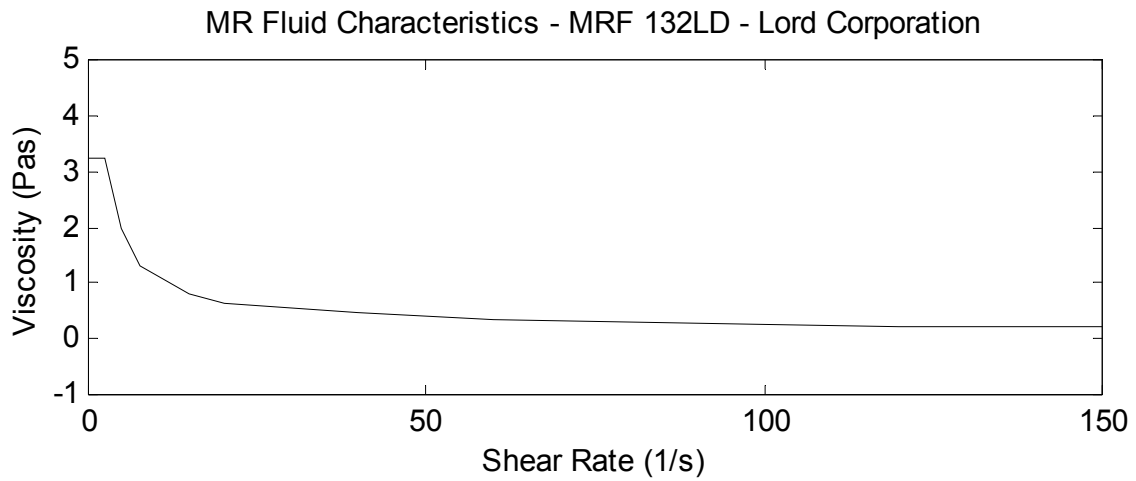


Figure 3.2. Viscosity as a function of shear rate.

The shear rate is proportional to the relative velocity between the compressor and the vehicle body. The shear rate is calculated by dividing the relative velocity (units of $\frac{m}{s}$) by the width of the gap (m), thus the shear rate has the dimensions of $\frac{1}{s}$.

Independent inquiries were made into the affect of temperature and magnetic field on the viscosity of MR fluid. In each case, information gathered led to the conclusion that the change in viscosity of the MR fluid due to temperature and magnetic field are negligible [7]. This model was used throughout this research.

The active component is derived from resistance due to yield stress, which is a function of the magnetic induction created by a coil that is incorporated into the isolator. Figure 3.3 gives an example of the yield stress as a function of magnetic induction.

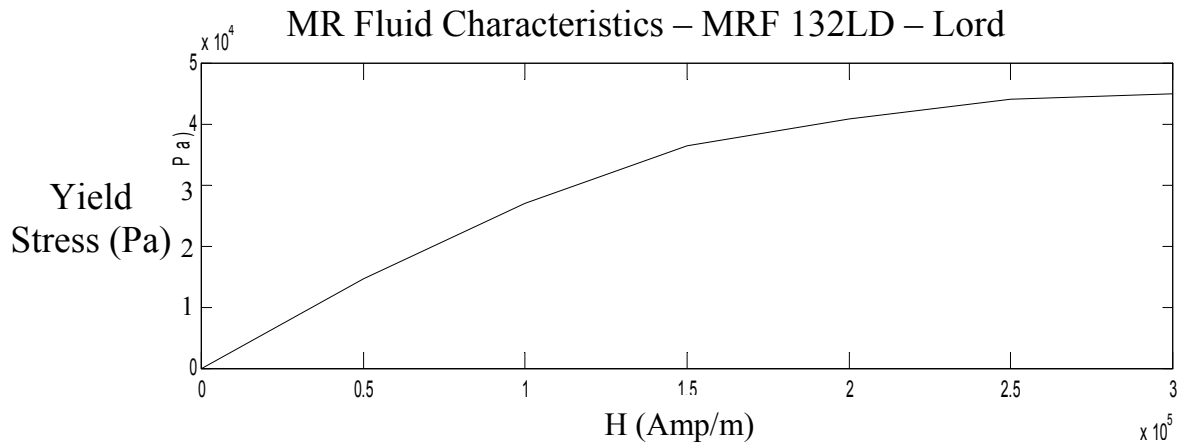


Figure 3.3. Yield stress as a function of magnetic induction.

3.3 MR Fluid Working Modes

MR fluid has three different types of working modes, depending on how the fluid is loaded. The three modes are shear, flow, and squeeze. Figures 3.4 to 3.6 illustrate how the fluid is worked in

each of the three different modes. Different equations are used to calculate the resistive force for each of the different modes.

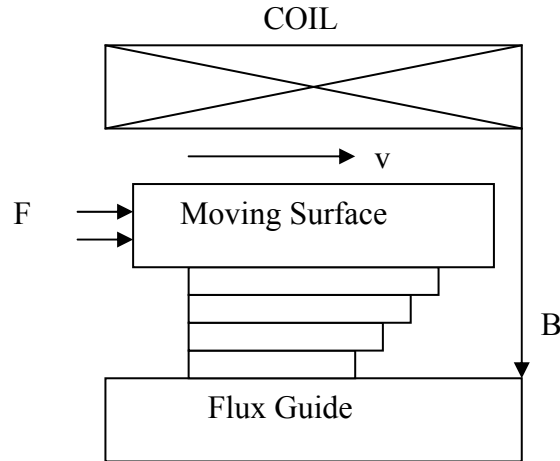


Figure 3.4. Working of a MR fluid in the shear mode. B is the magnetic flux direction.

The shear mode works when one surface moves through the fluid with respect to another surface. The magnetic field is perpendicular to the direction of motion. A MR based clutch is a good example of working the fluid in shear mode [8]. The equation corresponding to the shear mode is:

$$f = \frac{SLb\eta}{h} + Lb\tau_y \quad (3.2)$$

where f is the resultant force based on the plate area [3].

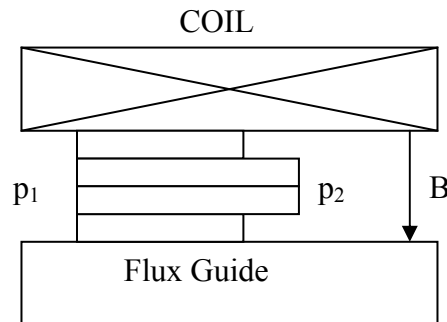


Figure 3.5. Working of a MR fluid in the flow mode. B is the magnetic flux direction.

The flow mode is characterized by two static flux guides with the magnetic field normal to the flow [8]. The magnetic field can be used to control flow resistance and pressure drop across the valve. Automotive shock absorbers work in the flow mode. The equation corresponding to the flow mode is [3]:

$$\Delta P = \Delta P_{0, HF} + \Delta P_{ER, HF} = \frac{12\eta QL}{bh^3} + 3\frac{L}{h}\tau_y \quad (3.3)$$

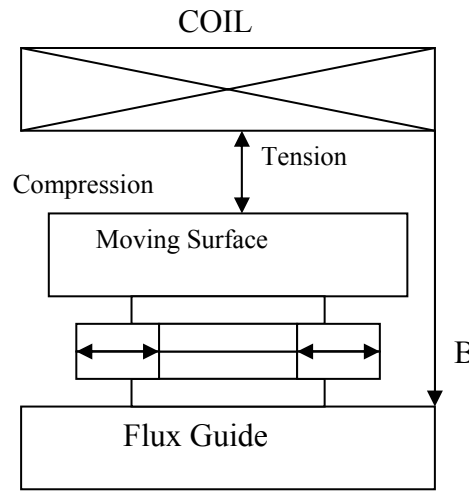


Figure 3.6. Working of a MR fluid in the squeeze mode. B is the magnetic flux direction.

The squeeze mode works when two parallel surfaces are used to compress the fluid. The magnetic field is parallel to motion of the surfaces. The magnetic flux density can be used to adjust the normal force to resist the motion. The squeeze mode has been shown to damp vibrations with high forces and low amplitudes. The equation corresponding to the squeeze mode is [9]:

$$F = \frac{2\pi\tau_0 a^3}{h_0 - h(t)} \Phi(x) \quad (3.4)$$

CHAPTER 4. MODELING THE ISOLATION SYSTEM

A single-degree of freedom model is used to model each system. The model simulates a compressor mounted to a vehicle body. To simplify the model, the motion of the vehicle body is modeled as a 1 Hz sine wave. This simulates the vehicle body bouncing at the natural frequency of the suspension system. Two seconds of data are simulated. Halfway through the model a speed bump is introduced. The speed bump is a severe test of the isolator's durability.

4.1 Simulation of the Passive Isolator

A simulation of the passive isolator was conducted first. The model was used to create baseline performance standards for an existing isolator, and to show passive trend lines when stiffness and damping parameters are changed. The model and associated equations can be seen below.

The algorithm developed for the simulation can be found in Appendix B.

The passive model can be seen in Figure 4.1. The model shows the compressor mounted to the vehicle body through an isolator that has only passive stiffness and passive damping components (k_{passive} and c_{passive} , respectively).

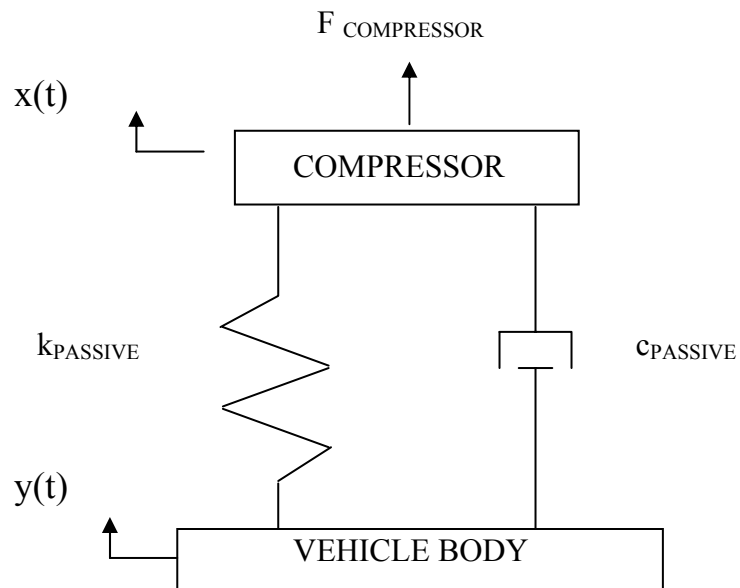


Figure 4.1. Passive model.

The free body diagram for the passive system can be seen in Figure 4.2. This diagram helps show how the equation of motion and the equation for transmitted force are developed.

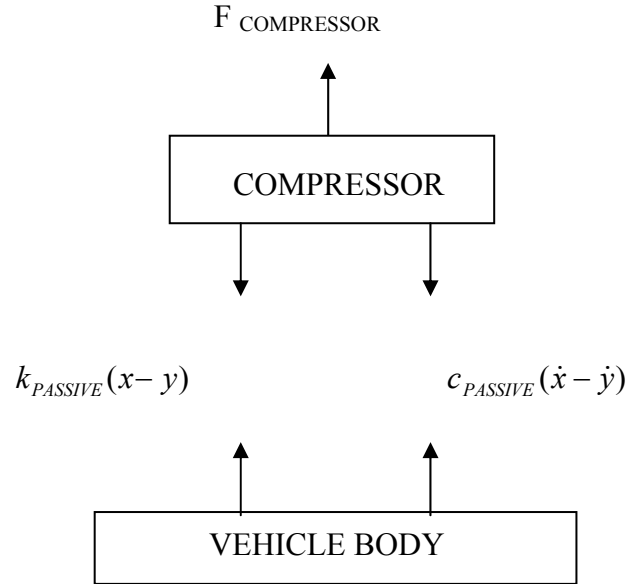


Figure 4.2. Passive free body diagram.

The equation of motion is created by summing the forces seen in the free body diagram, given by:

$$+\uparrow \sum F = m\ddot{x} \quad (4.1)$$

This summation of forces is:

$$m\ddot{x} = -k_{PASSIVE}(x-y) - c_{PASSIVE}(\dot{x}-\dot{y}) + F_{COMPRESSOR} \quad (4.2)$$

Rearranging gives:

$$m\ddot{x} = k_{PASSIVE}y - k_{PASSIVE}x + c_{PASSIVE}\dot{y} - c_{PASSIVE}\dot{x} + F_{COMPRESSOR} \quad (4.3)$$

The acceleration of the compressor, \ddot{x} , is then calculated as:

$$\ddot{x} = \frac{1}{m} [k_{PASSIVE}(y-x) + c_{PASSIVE}(\dot{y}-\dot{x}) + F_{COMPRESSOR}] \quad (4.4)$$

This acceleration equation is put in the integration loop, which will be discussed in Section 4.5.

The force transmitted into the vehicle body is also seen in the free body diagram. A transmitted force is considered any force created from the relative motion between the vehicle body and the compressor that acts upon the vehicle body. The transmitted force is computed using:

$$+ \uparrow \sum F = F_{TRANS} \quad (4.5)$$

Including the spring and damper force in (4.5) gives:

$$+ \uparrow \sum F = F_{TRANS} = k_{PASSIVE}(x - y) + c_{PASSIVE}(\dot{x} - \dot{y}) \quad (4.6)$$

The compressor assembly, seen in Figure 1.1, consists of three baseline isolators and the compressor. This assembly is a production leveling compressor system. Each isolator is a simple passive isolator made of a synthetic rubber material of 60 durometer. The isolator was rated to withstand temperatures up to 110 °C. Testing showed the isolator to have a stiffness of $k=50,000$ N/m, and a damping ratio of $\zeta=0.1$. The damping coefficient of the isolator will change with temperature and frequency and is expected to have a minor effect on the performance of the isolator. The constant value is assumed for all the analyses in this thesis. The isolator has a height of 20 mm and outer diameter of 14 mm. It has a mass of 6.8 grams. The compressor assembly is 230 mm long, 180 mm wide, and 110 mm tall. The compressor had a mass of 3 kg (6.6 lb). For the model, it was assumed that one-third of the mass (1 kg) was on each isolator.

4.2 Simulation of the Semi-Active Isolator

Once the passive system was modeled, a MR fluid based semi-active isolator was modeled to replace the passive isolator. The fluid was modeled as a Bingham plastic, where there is a passive and active component to the fluid. The equations used to model the fluid are as follows [3]:

$$F_{MR} = f_{yield} + c_{MR}(\dot{x} - \dot{y}) \quad (4.7)$$

$$\tau_{MR} = \tau_y + \eta\dot{\gamma} \quad (4.8)$$

The c_{MR} component of the fluid is the passive part of the fluid. It is a function of the viscosity of the fluid, η , the shear rate of the fluid, $\dot{\gamma}$, and the geometry of the flow path. The shear rate of the fluid is a function of the relative velocity and fluid gap width. Also, the viscosity of the fluid is a function of the shear rate [10].

The f_{yield} is the active isolation component of the MR fluid. It is a function of the yield strength of the fluid, τ_y . The yield stress of the MR fluid is related to the resistance force through the gap area of the isolator's flow channels and the strength of the magnetic field surrounding it. The model and equation relationships can be seen below. The use of acceleration or relative velocity will be discussed in Section 4.5.

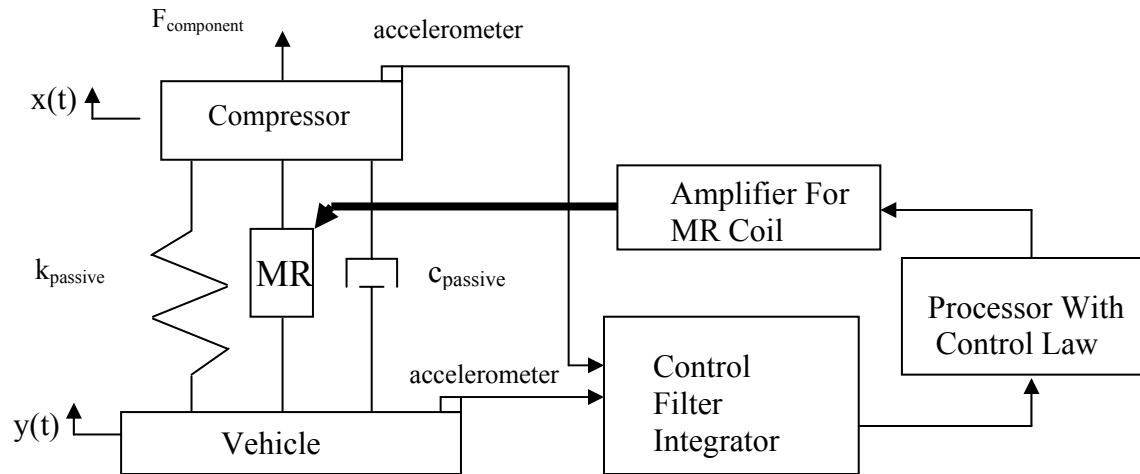


Figure 4.3. Semi-active model of the MR isolator.

The free body diagram for the semi-active system can be seen in Figure 4.4. Once again, the diagram helps show how the equation of motion and the equation for transmitted force are developed. The model is identical to the passive model, with the addition of the force created by the MR fluid.

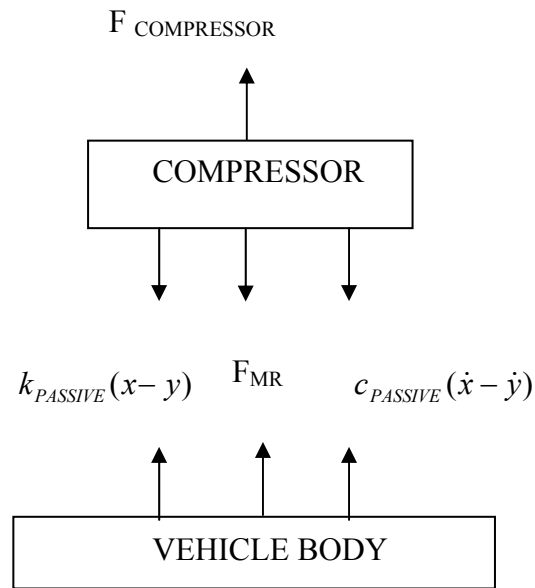


Figure 4.4. Semi-active free body diagram.

The equation of motion for the semi-active system is very similar to the passive equation. It is once again created by summing the forces seen in the free body diagram.

$$+\uparrow \sum F = m\ddot{x} \quad (4.9)$$

However, in the semi-active system, the forces created by the MR fluid are included in the equation of motion, as:

$$+\uparrow \sum F = m\ddot{x} = -k_{\text{PASSIVE}}(x-y) - c_{\text{PASSIVE}}(\dot{x}-\dot{y}) - F_{\text{MR}} + F_{\text{COMPRESSOR}} \quad (4.10)$$

The summation is:

$$m\ddot{x} = k_{PASSIVE}y - k_{PASSIVE}x + c_{PASSIVE}\dot{y} - c_{PASSIVE}\dot{x} - F_{MR} + F_{COMPRESSOR} \quad (4.11)$$

The acceleration of the compressor is then calculated as:

$$\ddot{x} = \frac{1}{m} [k_{PASSIVE}(y - x) + c_{PASSIVE}(\dot{y} - \dot{x}) - F_{MR} + F_{COMPRESSOR}] \quad (4.12)$$

The transmitted force equation is also very similar to the passive equation:

$$+ \uparrow \sum F = F_{TRANS} \quad (4.13)$$

But once again, the forces generated by the MR fluid need to be considered:

$$+ \uparrow \sum F = F_{TRANS} = k_{PASSIVE}(x - y) + c_{PASSIVE}(\dot{x} - \dot{y}) + F_{MR} \quad (4.14)$$

It is important to note that the MR force is transmitted to the vehicle body. For this reason, the control of the MR fluid is very important. This is discussed in Sections 4.4 and 4.5.

To generate the passive and active force components from the MR fluid, the pressure drop through the isolator must be analyzed. For flow mode, the pressure drop given by [3]:

$$\Delta P = 3 \frac{L}{h} \tau_y + 12 \frac{\eta Q L}{bh^3} \quad (4.15)$$

From this equation, the force components can be derived using the area of the flow channel, A_{gap} , and the area of the isolator plunger, A_i . The final design of the isolator will be discussed in Chapter 8, but for now, these areas will be used. The derivation of the active component follows:

$$f_{yield} = A_{gap} 3 \frac{L}{h} \tau_y = 3\pi(r_o^2 - r_i^2) \frac{L}{h} \tau_y \quad (4.16)$$

It is important to note that the active component of the MR fluid is directly proportional to the yield stress of the fluid.

The derivation of the passive component is a little more complicated. The passive force is related to the viscosity and the flow rate as:

$$c_{MR}(\dot{x} - \dot{y}) = 12 \frac{\eta QL}{bh^3} \quad (4.17)$$

However, the flow rate is a function of the relative velocity, thus:

$$c_{MR}(\dot{x} - \dot{y}) = 12 A_{gap} \frac{\eta QL}{bh^3} = 12 A_{gap} \frac{\eta A_i (\dot{x} - \dot{y}) L}{bh^3} = 12 \pi (r_o^2 - r_i^2) \frac{\eta \pi r_i^2 (\dot{x} - \dot{y}) L}{bh^3} \quad (4.18)$$

When the relative velocity is factored out, the passive component is seen as being proportional to the viscosity of the fluid and the geometry of the isolator, and is:

$$c_{MR} = 12 \pi (r_o^2 - r_i^2) \frac{\eta \pi r_i^2 L}{bh^3} = 12 \pi r_i^2 \pi (r_o^2 - r_i^2) \frac{\eta L}{bh^3} \quad (4.19)$$

Simplifying:

$$c_{MR} = 12 A_i A_{gap} \frac{\eta L}{bh^3} \quad (4.20)$$

Combining the passive rubber components and the MR components of the isolator, the MR based isolator is modeled as follows:

$$F_{Dampner} = k(x - y) + (c + c_{MR})(\dot{x} - \dot{y}) + f_{yield} \quad (4.22)$$

where c and k were again passive properties of the isolator, and, f_{yield} and c_{MR} are the active and passive components of the MR fluid derived in (4.16) and (4.20), respectively.

The control of the f_{yield} component is very important. The goal of the f_{yield} term is to control vibration occurring at road input frequencies without transmitting the higher frequency created by the compressor. This is to be done by controlling the active MR component to model the passive damping provided by the isolator, but using a low pass filter to eliminate the higher frequencies created by the compressor.

4.3 System Inputs

The compressor is turned on and off during the simulation. The unbalance force due to the compressor rotation is simulated as a sinusoidal force input to the compressor mass. The algorithm for this input is given in Appendix E. The vehicle body motion is modeled as a body heave mode, with a speed bump input midway through the simulation. This algorithm can also be seen in Appendix E. These model inputs are displayed in Figure 4.5, and are used as the inputs for all models.

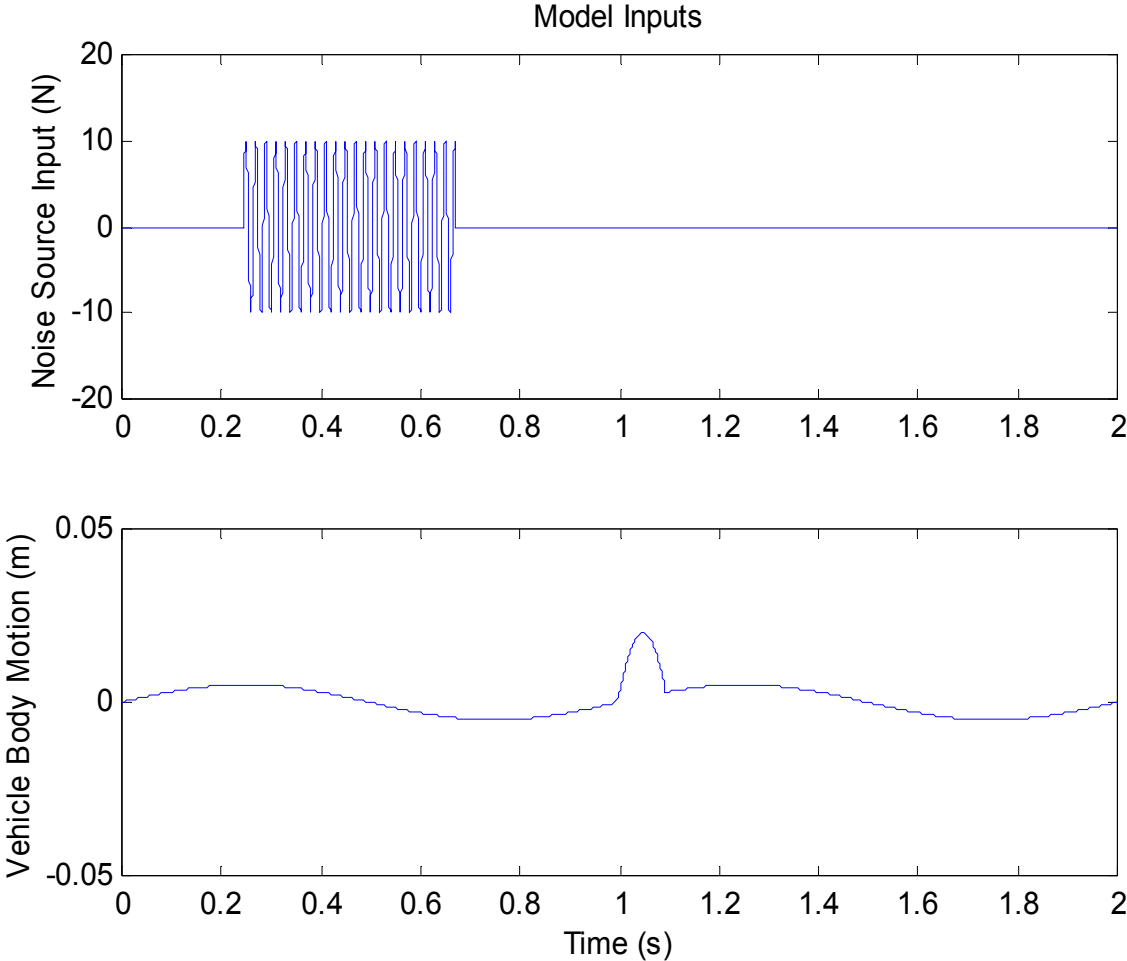


Figure 4.5. Model inputs for the compressor and vehicle body.

4.4 System Outputs

The main outputs from the simulation are,

1. Power spectral density of the transmitted force at 50 Hz, the frequency of the compressor. The PSD was calculated during the time period that the compressor is on. The PSD was computed from the single time signal. There was no random signal where averaging was needed. An example of the PSD is seen in Figure 4.6.

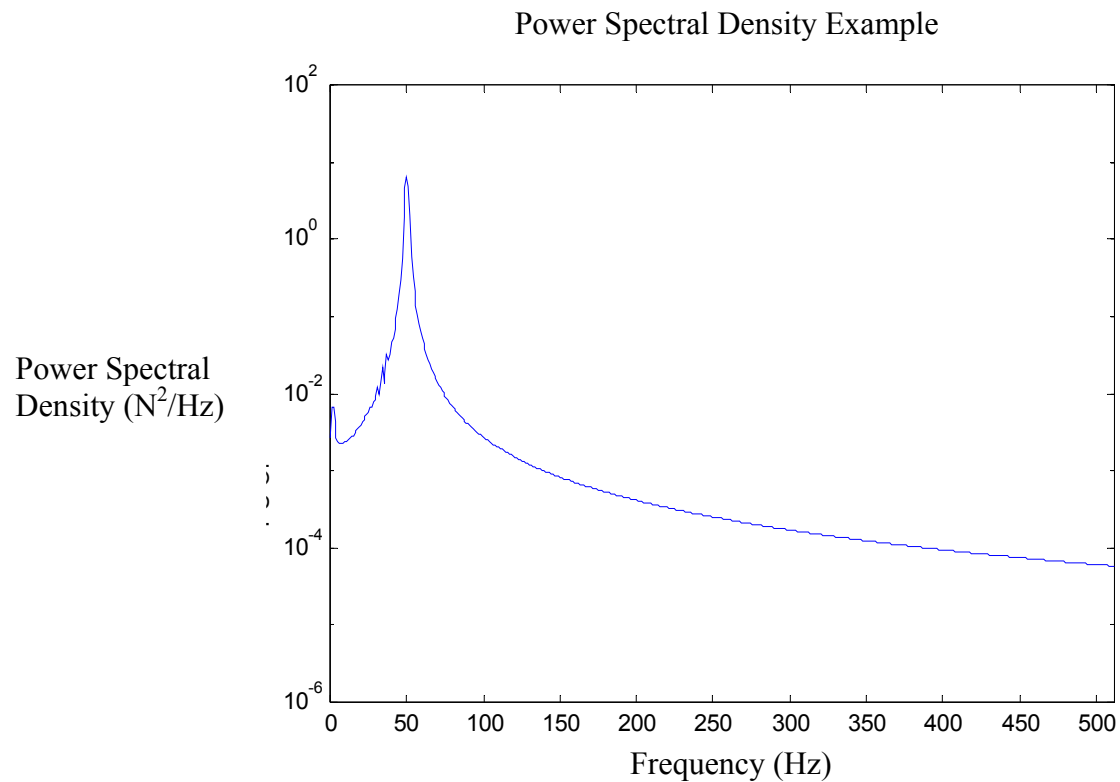


Figure 4.6. Example of power spectral density plot.

2. Maximum relative displacement between the compressor and the vehicle body. This occurs shortly after the bump. This is considered as a measure of durability of the isolator.

4.5 Newmark-Beta Explicit Time Integration Method

A Newmark-Beta explicit time integration method with force balance iteration was used to move from one time point to the next because the equations of the isolator system are nonlinear and cannot be solved in closed form. The integration method requires initial displacement, velocity, and acceleration components. It then calculates displacement and velocity for the next time point, and inputs them into equation of motion. Here, the acceleration component is calculated. Ten iterations are run for each time point, allowing the calculations to converge. Once convergence has been met, the loop is repeated for the next data point. This is an accurate, flexible and simple method for solving nonlinear equations. This method improves the convergence of the iteration, however a small time step is required [11].

4.6 Filter Design

The low-pass filter was designed as a second order Butterworth filter. The filter was designed with a cutoff frequency of 30 Hz in order to “turn off” the actuator at 50 Hz so the compressor vibration is not transmitted to the automobile frame, which causes a noise that annoys passengers. The following amplitude and phase characteristics were seen with this filter.

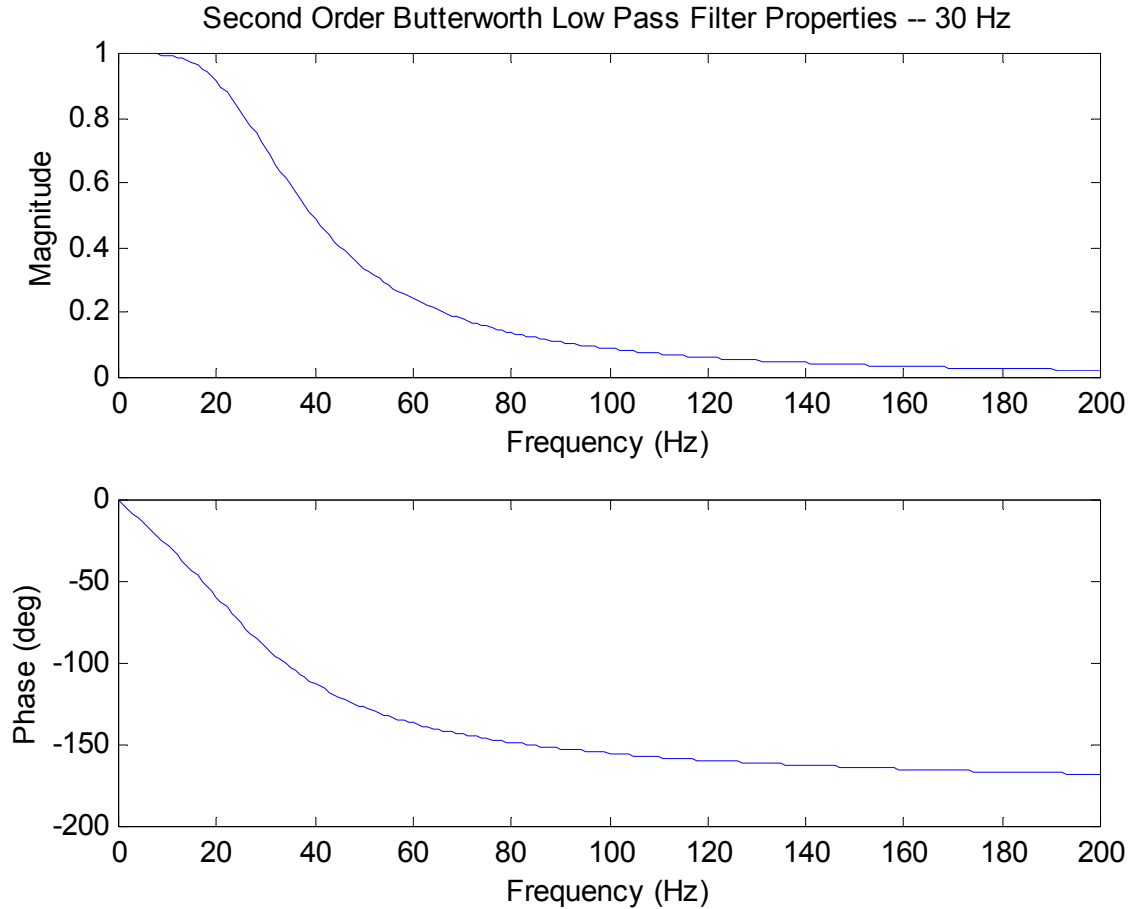


Figure 4.7. Characteristics of a second order Butterworth filter.

Figure 4.7 shows how the filter introduces amplitude distortion based on frequency. It also shows how the filter introduces phase lag into the response of the active MR component. The phase lag from the filter increases as the natural frequency of the isolator increases. A higher order filter would provide a sharper cut-off, but would increase phase lag [12]. A second order filter was found to provide the best compromise between attenuation and phase lag for this problem. The following demonstration shows how the phase lag hinders results.

In the algorithm seen in Appendix E, the active variable v is set equal to the relative velocity between the compressor and the structural base. It is then filtered, producing a variable z with the compressor excitation content removed. The variable z is then scaled to produce the

yield stress of the fluid. The variable v is exactly in phase with passive isolation force. If the filter was a perfect filter, there would be no phase lag in variable z , and it too would be exactly in phase with the passive isolation force. However, as seen in Figure 4.8, when the vehicle hits the bump, the response of the active component (blue line) lags behind the passive component (red line) by roughly ninety degrees. Because the active component lags, it cannot be as effective as possible. If the amplitude of the active MR component is scaled too high, this phase lag can induce instability in the system.

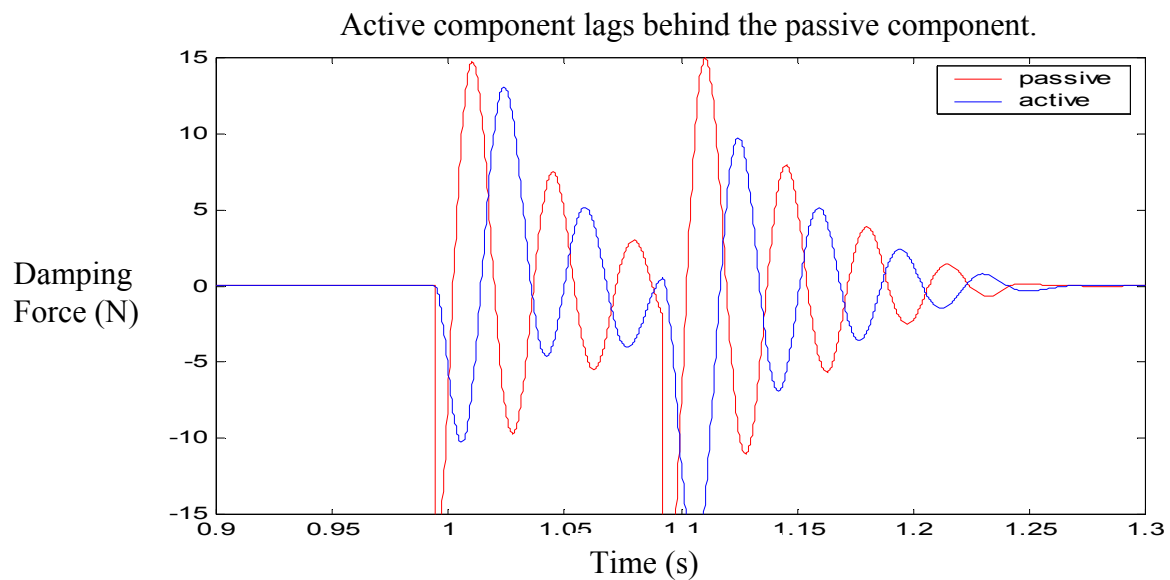


Figure 4.8. Showing the phase lag with a Butterworth low pass filter.

Several ideas were explored for try to resolve this phase lag issue and improve results. One idea is that the phase lag can be corrected by the introduction of a phase lag compensator. Displacement and velocity feedback control with phase lag can be resolved into corrected displacement and velocity components. This feedback can be used in a linear control law, as

discussed by Soong [13]. The limitation of this technique is that both position and velocity feedback are needed.

Another idea was the concept of an ideal filter. It is thought that this would be best for this situation. This filter would have no phase lag at any frequency, and the amplitude cut-off is perfect at the cut-off frequency. The characteristics of a perfect filter are seen in Figure 4.9.

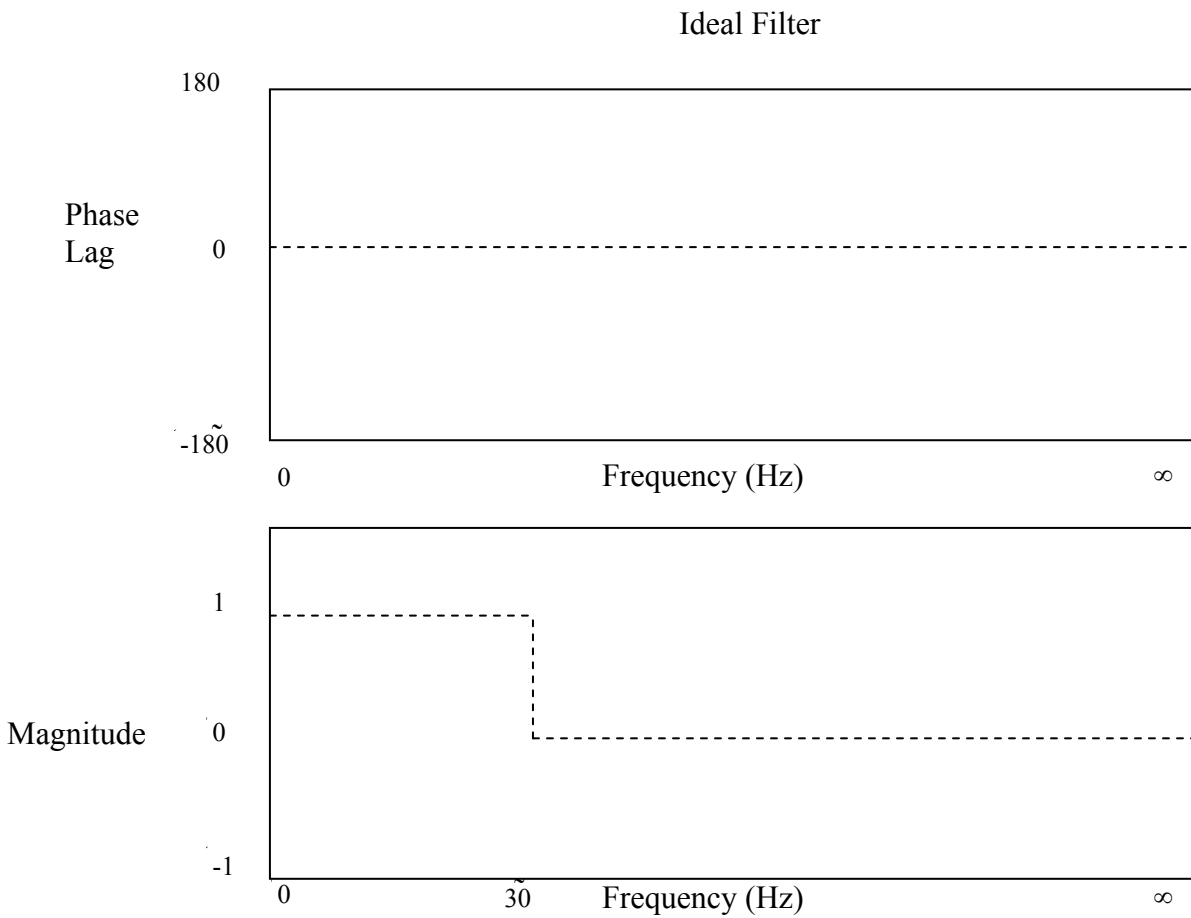


Figure 4.9. Characteristics of an ideal low-pass filter.

To get the desired results for this type of control system, research showed that the design of the low pass filter is a very important factor. With a filter that introduces phase lag, phase lag induced instability becomes possible. However, research showed compensating for the filter lag is very difficult. While the subject needs further research, a simpler approach was taken for this model.

To illustrate the adverse affects of the low pass filter, the filter was simply turned off when the compressor was off. The filter was there for the sole purpose of taking out the component in the relative velocity response due to the compressor. If the compressor is not running, there is no high frequency sinusoidal excitation. Therefore, there is no reason to have the filter on. With the filter off, the active component is in phase with the passive component when the vehicle hits the bump, as seen in Figure 4.10.

The active component is in phase with the passive component.

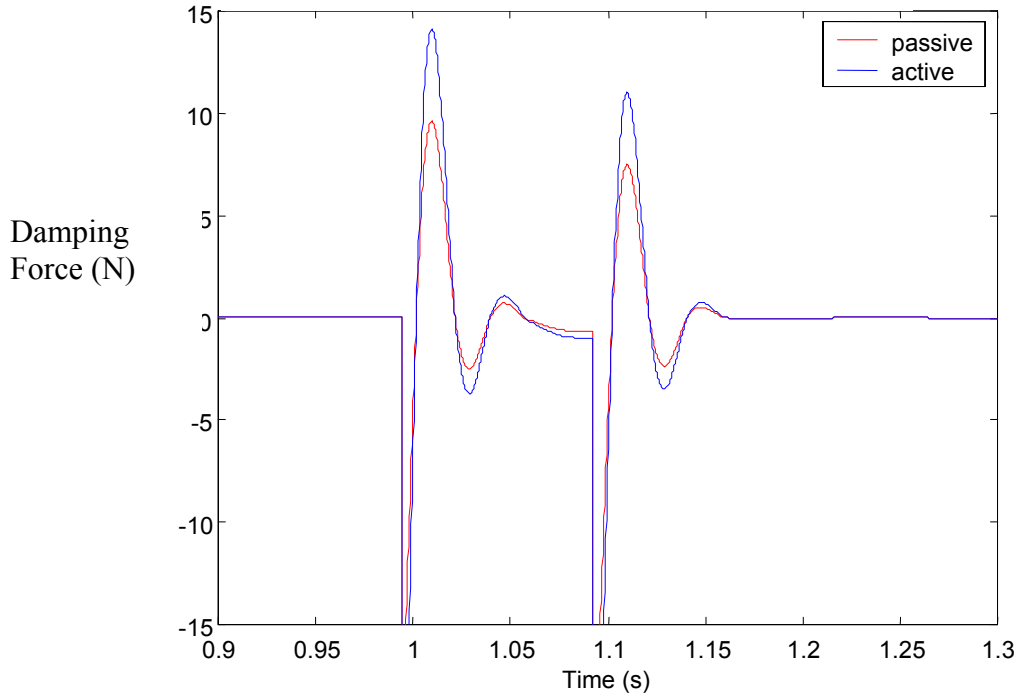


Figure 4.10. Reaction of isolator components with filter off.

4.7 Control Law Design

The semi-active isolator is basically a damper with static and viscous components, and the static component (F_{yield}) can turn on an off and change its force through electronic control. Different possible control laws for the static component were considered.

Skyhook control is a method based on minimizing the vibration velocity of the component in inertial space. It is a simple method used, for example, in a semi-active suspension to minimize the vibration of automobile bodies due to road inputs, and to minimize the vibration acceleration of buildings due to earthquake inputs.

Relative velocity control, defined here, is a control law based on minimizing the vibration velocity of the component relative to the input frame. This is also a simple method and would minimize the relative displacement of the compressor relative to the automobile body. In this approach, increasing the control action of the isolator (making the isolator very stiff with high damping) would reduce the relative vibration but increase the transmitted force.

A third approach, force transmitted control, defined here, would minimize the force transmitted through the isolator to the body of the automobile. This would require measuring the relative displacement and relative velocity and it would also require models of the isolator. This approach is more complex, and the isolator properties may change causing the control to become less efficient. Alternately, a force transducer might be used between the isolator and body, but this would increase the size and cost of the isolator. The force transmitted control, alone, would tend to make the isolator become very soft so that no force is transmitted. An optimal control law probably would have to include the force transmitted and the relative displacement components.

A goal of the isolator design is also to make the isolator and control system simple. Therefore, a skyhook control algorithm, seen in Figure 4.9, was simulated first for the control of the isolator. The skyhook control is used to minimize the vibration of components in inertial space. It is based on the following logic:

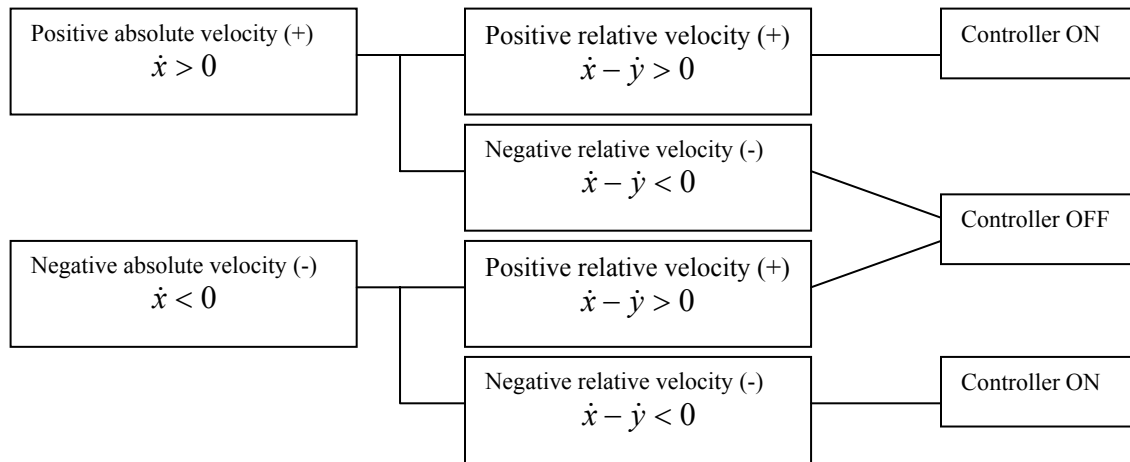


Figure 4.11. Diagram of skyhook control law.

When simulated, this algorithm tried to control the compressor with respect to inertial space. A careful evaluation of the results showed that the active MR component would not react immediately to the bump in the model. This can be seen in Figure 4.12 where a 10 ms lag occurs in starting the yield force component of the control. The viscous damping passive term reacts immediately as it should.

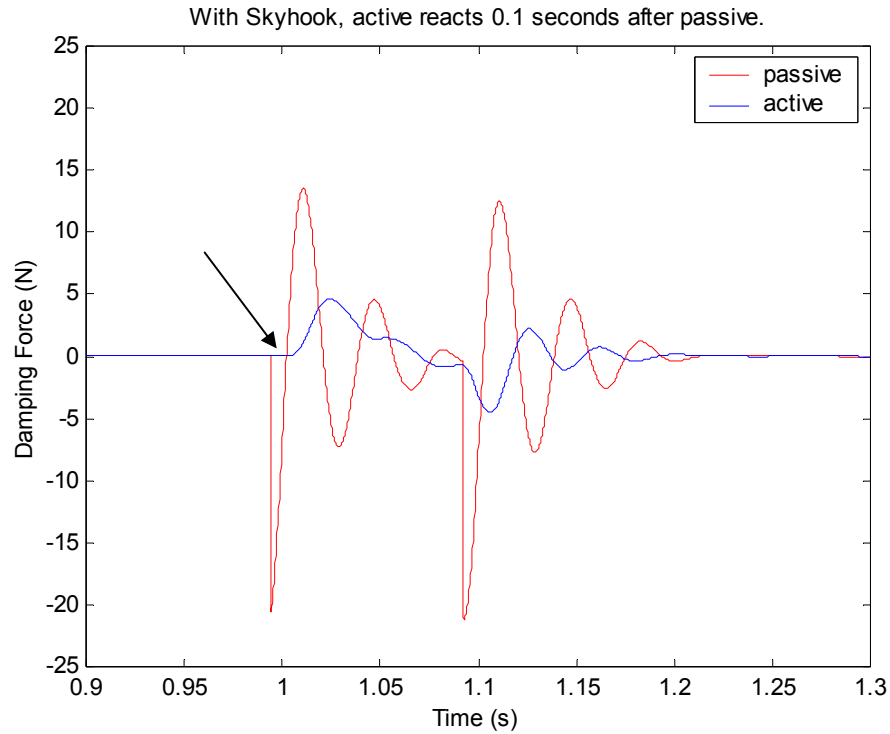


Figure 4.12. Skyhook control law does not allow the isolator to react properly to a bump.

Controlling the vibration of the compressor relative to the base is important for durability. Thus a relative velocity control or relative skyhook control was investigated. This control would replace the velocity component with the relative velocity component. The algorithm is seen in Figure 4.13.

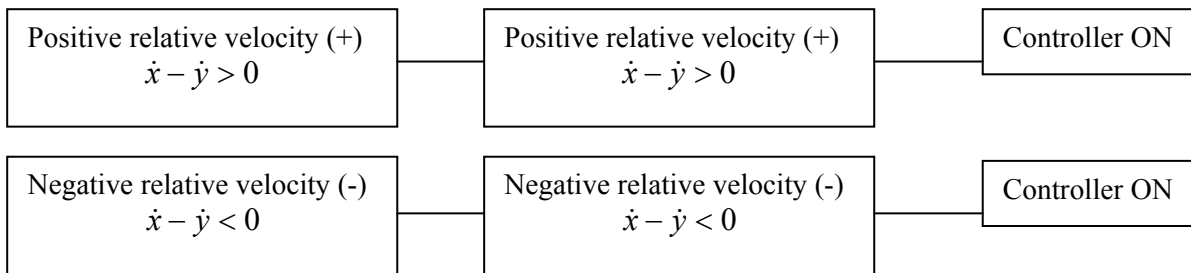


Figure 4.13. Diagram of relative skyhook control law.

It was quickly noted that this control was the same as always having the control on, since the logic looked at the square of the relative velocity, and the square of any number is always positive. The results without the skyhook control can be seen in Figure 4.14 where both the viscous and yield force terms of the control act at once.

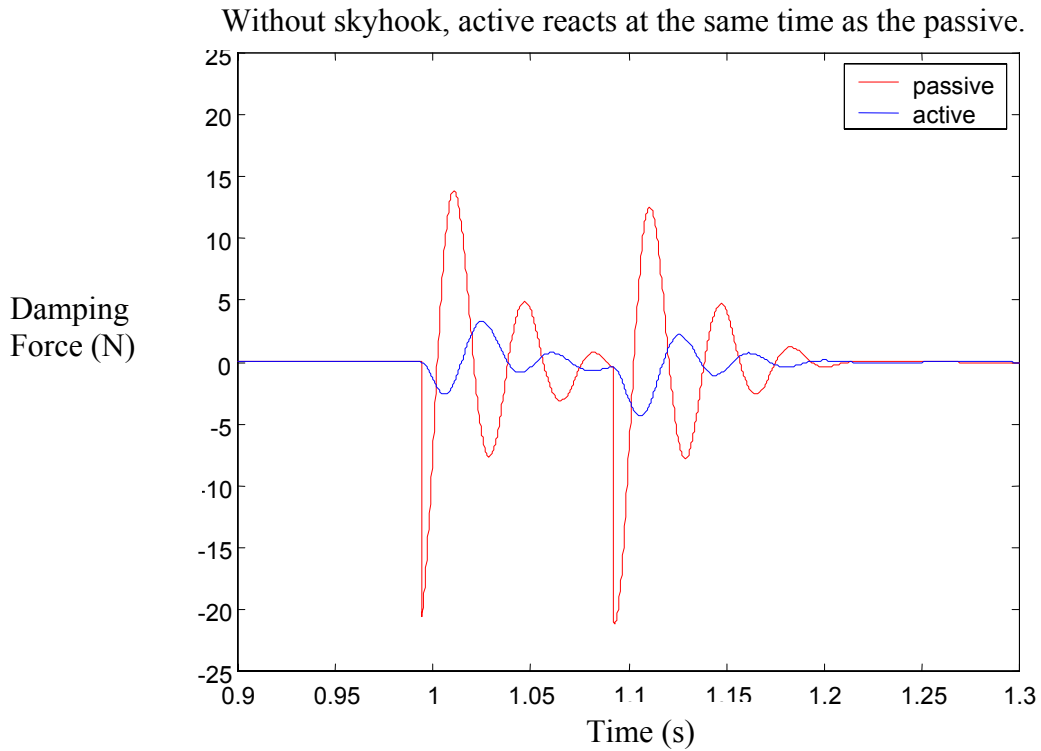


Figure 4.14. No skyhook control allows the isolator to react properly.

In the control system shown in Figure 4.3, an accelerometer is located on the mass (compressor) and another accelerometer is located on the base (auto body). The acceleration signals can be integrated and then subtracted to give the velocity of the mass relative to the base. This relative velocity is used as the feedback signal in the control algorithm. While this approach

is feasible, the two channels of data acquisition and the signal processing (integration) would add complication and cost to the isolator system.

Another approach is to design a direct relative velocity sensor built into the isolator. The velocity of the piston in the isolator with respect to the base is the relative velocity that must be measured. It may be possible to have a magnet built into the piston rod and a small coil of wire attached to the isolator housing which is attached to the base. The magnet moving through the coil of wire around the piston rod will produce a voltage in the coil that will be proportional to the velocity of the magnet relative to the coil. This is a simple inductive non-contact sensor. Linear Variable Differential Transformers [14] are similar devices used to measure relative displacement and these may be adapted to measure velocity, or the derivative of the relative displacement may be taken to obtain relative velocity. A design with a sensor in each isolator would have the added possibility and advantage of individually controlling each isolator. This would provide rotational isolation for the component and is a potentially simple approach to achieve multi-degree-of-freedom control. The development of the sensor integrated within the isolator and multi-axis semi-active control are promising ideas that should be investigated and are suggested for future work.

4.8 Design of the MR Isolator

Once the control and filter issues were resolved, a fluid was chosen with the model. Lord Corporation's web site [10] was used to get fluid properties on their product MRF 132LD. This fluid was chosen because it had low viscosity properties. A fluid with higher viscosity would cause the passive component to control the compressor rather than the active component. This would make very inefficient use of the MR fluid.

Using the fluid properties, the size of the isolator to obtain the performance necessary was determined (radii, height, etc.) The power capability and coil design needed to generate the power could also be determined. With this done, the final design parameters could be determined (weight, size, fluid volume, coil length, etc) by running the simulations.

The semi-active results were compared to the passive results. The goal is to show that the semi-active design can give the same maximum relative displacement as the passive baseline, but, in addition, provide a significant reduction in noise transmission.

CHAPTER 5. ISOLATOR SIMULATION STUDIES

This chapter presents results of the simulations that were performed using the model of the isolation system developed in Chapter 4.

5.1 Results for the Passive Isolator Design

Figures 5.1 and 5.2 show the results generated from the single degree of freedom isolator model. Maximum relative displacement and the power spectrum of the transmitted force at 50 Hz are plotted against stiffness. A damping ratio of $\zeta = 0.1$, common for natural rubber, was used with each stiffness.

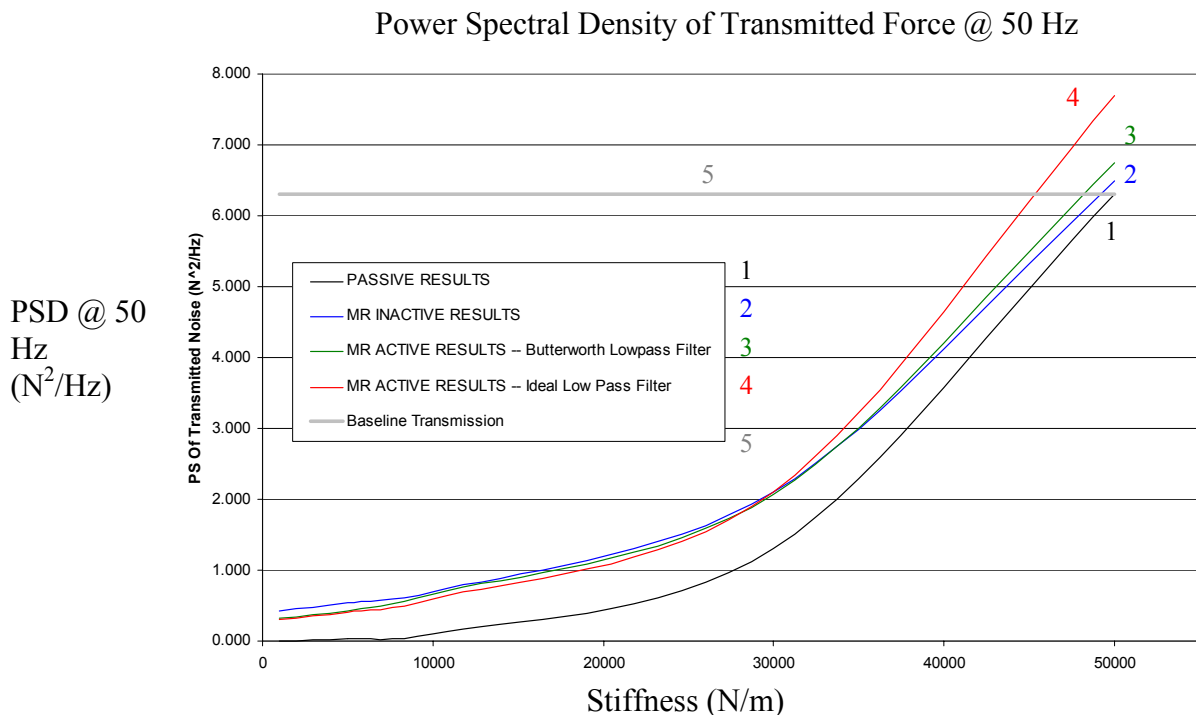


Figure 5.1. The effect of passive stiffness seen on transmitted force.

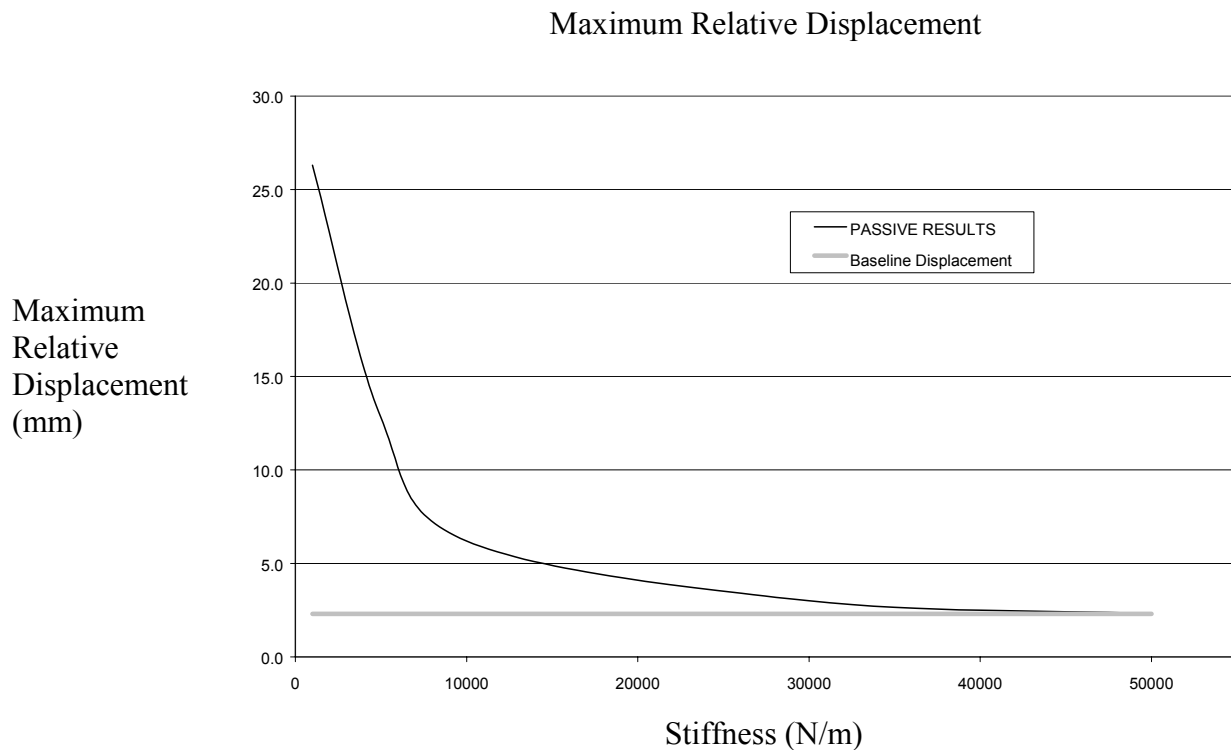


Figure 5.2. The effect of passive stiffness on maximum relative displacement.

The tradeoff between relative displacement and transmitted force can be seen. In Figure 5.1, an increase in stiffness results in increased transmitted force. However, in Figure 5.2, the increase in stiffness lowers relative displacement significantly. Also, the baseline performance is set. The goal of the MR based semi-active isolator is to improve upon the following results.

- (i) Maximum relative displacement of 2.3 mm.
- (ii) Maximum transmitted force spectral density from the compressor of $6.3 \text{ N}^2/\text{Hz}$.

5.2 Results for the Semi-Active Isolator

Figures 5.3 and 5.4 show the results generated from the single degree of freedom model.

Maximum relative displacement and the power spectrum of the transmitted force at 50 Hz are plotted against stiffness. $Zeta = 0.1$, common for natural rubber, was used with each stiffness.

The figures here include results from four designs:

- | | |
|---------------|--|
| Design Case 1 | Passive rubber isolator.

Case 1 models the isolator as seen in Figure 4.2. |
| Design Case 2 | Passive rubber isolator with passive MR fluid.

Case 2 models the isolator as seen in Figure 4.4. However, the active component of the MR fluid is turned off. Thus the force from the active component is zero. |
| Design Case 3 | Passive rubber isolator with active MR fluid w/ Butterworth filter.

Case 3 models the isolator as seen in Figure 4.4. A Butterworth second order filter is incorporated into the control of the active component of the MR fluid. Thus phase lag is introduced in this component. |
| Design Case 4 | Passive rubber isolator with active MR fluid w/ filter off.

Case 4 models the isolator as seen in Figure 4.4. The filter is turned off when the compressor is turned off. Therefore, there is no phase lag in the active component. |

Power Spectral Density of Transmitted Force @ 50 Hz

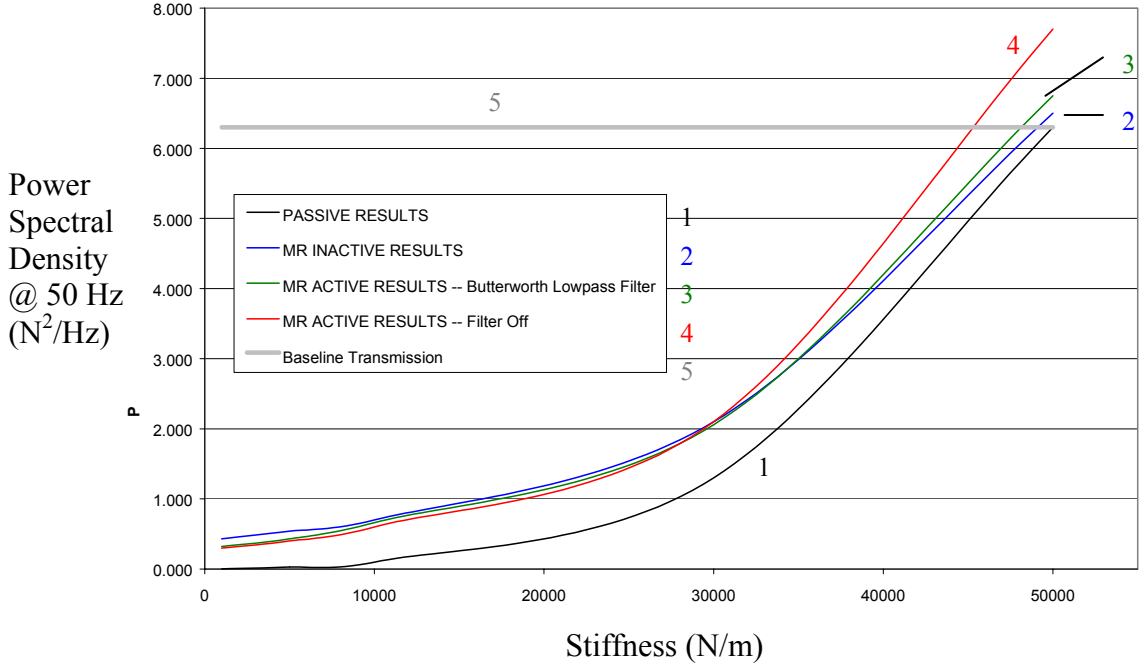


Figure 5.3. Transmitted force from the semi-active system.

Maximum Relative Displacement

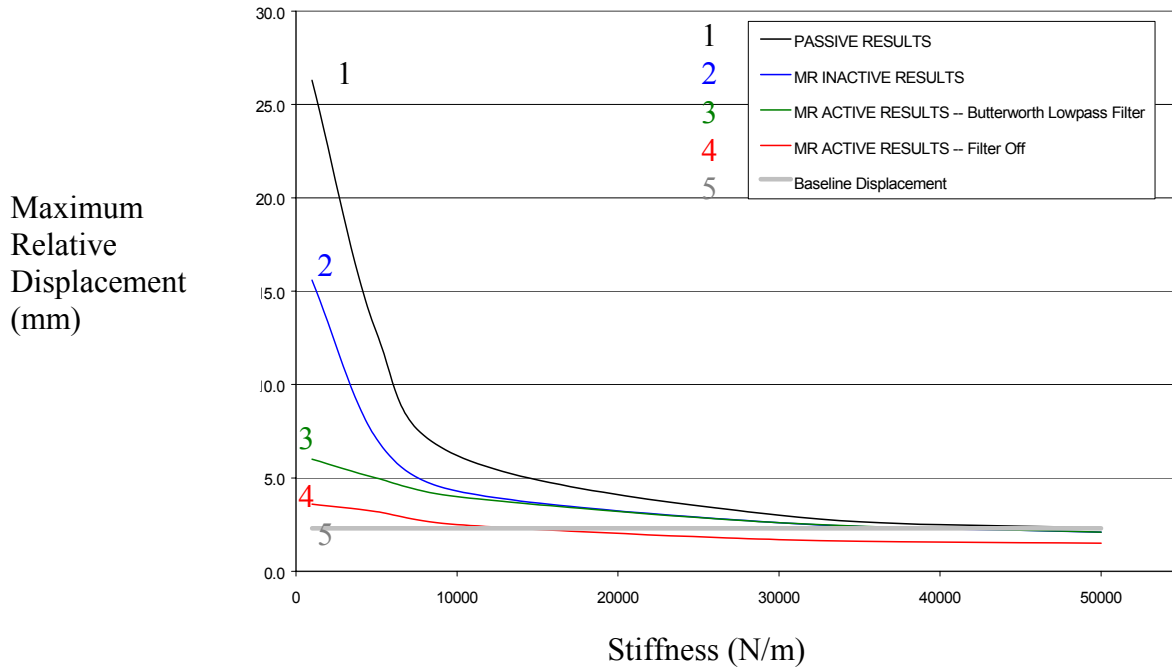


Figure 5.4. Maximum relative displacement results from semi-active system.

In these results, it can be seen that the passive component of the MR changes the results considerably. The maximum relative displacement is reduced, and the transmitted noise increases. When the active component is introduced with the Butterworth filter, the maximum relative displacement at low stiffness is reduced, however, there is little affect at higher stiffness. The transmitted noise is not affected much by the active component.

However, when the filter is turned off, the active fluid is in phase and the results improve significantly. Once again, the transmitted force is not affected, but the maximum relative displacement is reduced for each value of stiffness.

Figure 5.5 gives an indication of how the MR fluid, both passive and active, helps limit relative displacement when the filter is turned off.

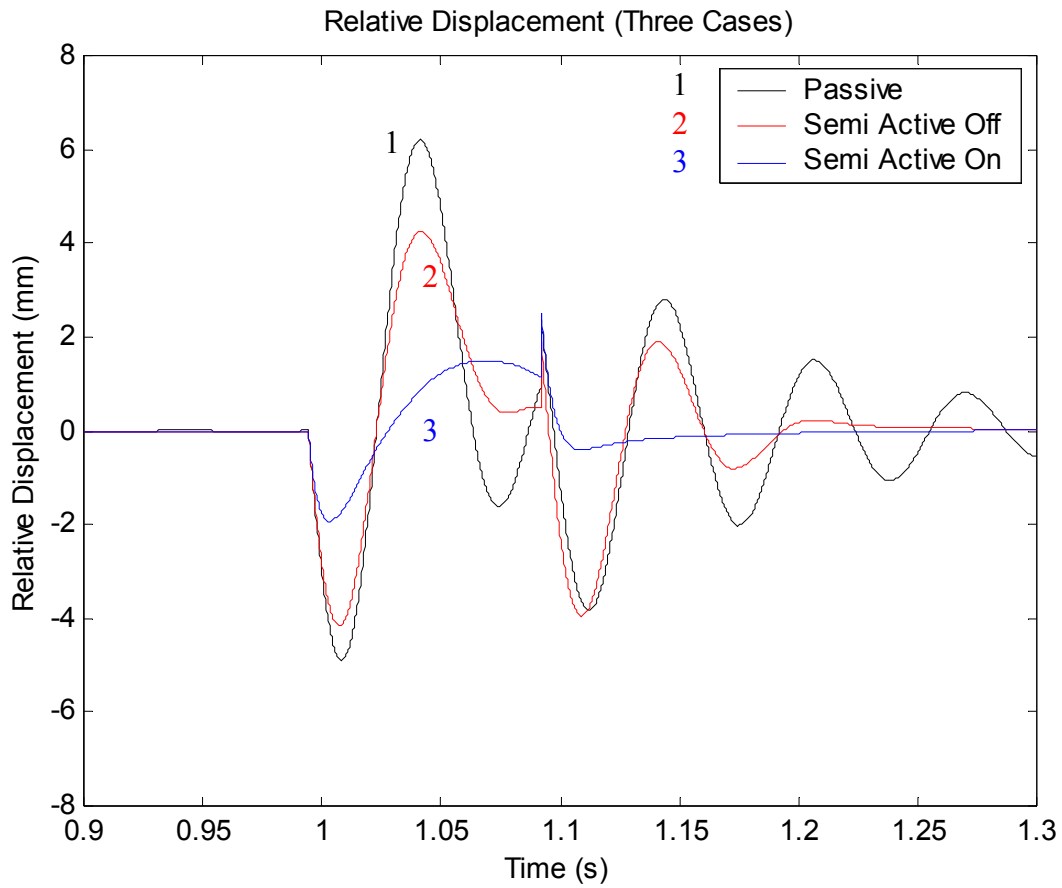


Figure 5.5. Improvement to relative displacement with MR fluid.

The results can be seen in tabular form below in Table 5.1. Shown in the table are the following properties: (i) isolator stiffness, (ii) isolator passive damping ratio, (iii) compressor mass per isolator, (iv) natural frequency of isolator, (v) maximum relative displacement, (vi) compressor transmitted force, and (vii) maximum forces seen by isolator components.

PASSIVE RESULTS					POWER SPECTRUM			MAXIMUM FORCES			
stiffness	mass	zeta	nat. freq.	scale	max. rel. displacement	comp. transmitted	spring	damper	passive fluid	active fluid	total
(N/m)	(kg)		(Hz)		(mm)	(N ² /Hz)	(N)	(N)	(N)	(N)	(N)
50000	1	0.1	35.6	0	2.3	6.300	113.7	26.6	0	0	116.0
30000	1	0.1	27.6	0	3.0	1.300	91.4	21.7	0	0	93.3
10000	1	0.1	15.9	0	6.2	0.100	62.0	11.9	0	0	62.9
5000	1	0.1	11.3	0	12.8	0.030	63.8	14.7	0	0	65.1
1000	1	0.1	5.0	0	26.3	0.003	26.3	5.0	0	0	27.7
MR INACTIVE RESULTS					POWER SPECTRUM			MAXIMUM FORCES			
stiffness	mass	zeta	nat. freq.	scale	max. rel. displacement	comp. transmitted	spring	damper	passive fluid	active fluid	total
(N/m)	(kg)		(Hz)		(mm)	(N ² /Hz)	(N)	(N)	(N)	(N)	(N)
50000	1	0.1	35.6	0	2.1	6.50	105.0	27.6	15.7	0	110.5
30000	1	0.1	27.6	0	2.6	2.10	79.2	21.1	15.5	0	84.5
10000	1	0.1	15.9	0	4.3	0.70	42.5	12.0	15.3	0	47.0
5000	1	0.1	11.3	0	7.1	0.54	35.5	11.5	20.9	0	42.0
1000	1	0.1	5.0	0	15.6	0.43	15.6	3.8	15.2	0	21.4
MR ACTIVE RESULTS -- Butterworth Lowpass Filter					POWER SPECTRUM			MAXIMUM FORCES			
stiffness	mass	zeta	nat. freq.	scale	max. rel. displacement	comp. transmitted	spring	damper	passive fluid	active fluid	total
(N/m)	(kg)		(Hz)		(mm)	(N ² /Hz)	(N)	(N)	(N)	(N)	(N)
50000	1	0.1	35.6	10000	2.1	6.75	104.4	27.4	15.6	7.4	112.4
30000	1	0.1	27.6	10000	2.6	2.06	78.4	21.5	15.8	8.8	88.0
10000	1	0.1	15.9	10000	4.0	0.66	40.2	13.4	15.2	50.4	56.7
5000	1	0.1	11.3	30000	5.0	0.43	24.8	11.5	20.6	56.4	80.5
1000	1	0.1	5.0	30000	6.0	0.32	6.0	3.8	17.1	13.7	57.8
MR ACTIVE RESULTS -- Ideal Low Pass Filter					POWER SPECTRUM			MAXIMUM FORCES			
stiffness	mass	zeta	nat. freq.	scale	max. rel. displacement	comp. transmitted	spring	damper	passive fluid	active fluid	total
(N/m)	(kg)		(Hz)		(mm)	(N ² /Hz)	(N)	(N)	(N)	(N)	(N)
50000	1	0.1	35.6	45000	1.5	7.70	75.7	26.7	15.2	121.6	158.5
30000	1	0.1	27.6	45000	1.7	2.10	49.6	20.9	15.3	122.5	152.9
10000	1	0.1	15.9	45000	2.5	0.60	25.2	12.2	15.5	124.1	144.7
5000	1	0.1	11.3	45000	3.2	0.40	15.7	8.5	15.2	121.7	141.4
1000	1	0.1	5.0	45000	3.6	0.30	3.6	3.7	14.8	118.4	136.9

Table 5.1. Summary of simulation results.

The maximum forces are shown in the right columns of the Table 5.1 and give an indication of how the forces seen by the different components of the isolator compare to each other. The columns are linked to the following forces:

- (i) Spring force resulting from the passive stiffness component k .
- (ii) Damper force resulting from the passive damping component c .
- (iii) Passive fluid force resulting from the passive component of the MR fluid.
- (iv) Active fluid force resulting from the active component of the MR fluid.
- (v) Total force resulting from the sum of all the isolator forces.

In Table 5.1, the results show the force resulting from the passive stiffness and damping components decreases as the passive stiffness of isolator decreases. This is why transmitted noise decreases when stiffness and damping decrease. However, the results also show the negative affect on relative displacement, and thus durability, when the stiffness decreases.

The active results show why turning the filter off is necessary. When the Butterworth low pass filter is used, the active component of the MR fluid is roughly the same size as the passive component of the MR fluid. If the active force is scaled higher than this, phase lag causes the maximum relative displacement to increase. If the active force is scaled high enough, the isolator will become unstable. Percentage of noise reduction for each case is seen below:

Inactive control with MR fluid	50%
Active control with Butterworth low pass filter	55%
Active control with filter off	83%

When the filter is turned off, the active component of the MR fluid is nearly eight times the force from the passive component. The fact that there is no phase lag allows the active MR component to be scaled in a manner where it can be really reduce the relative displacement. Figure 5.6 shows all four isolator components with the filter turned off, along with the relative displacement of the compressor.

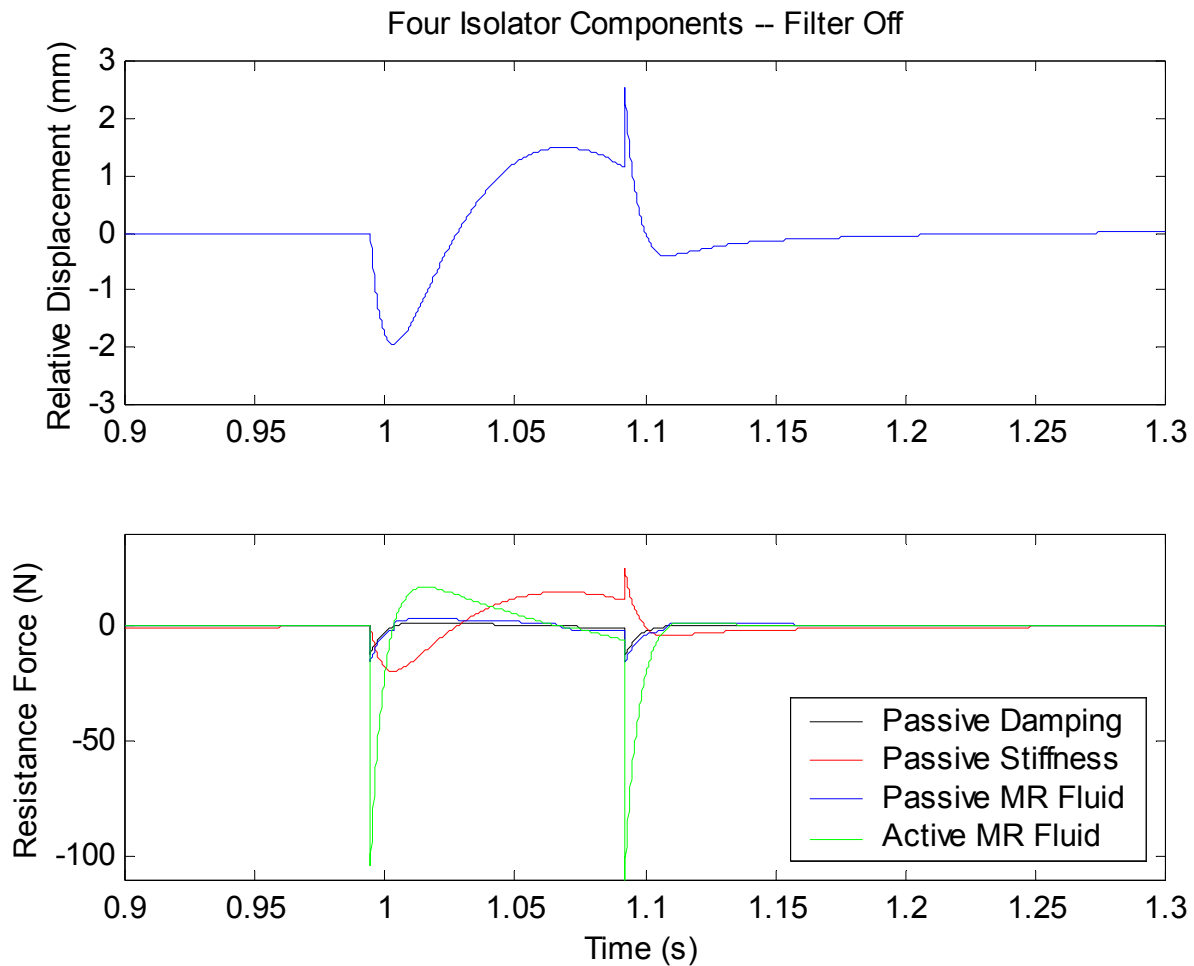


Figure 5.6. Relative displacement and isolator force components with filter off.

A look at the MR fluid viscosity yields another interesting result. As mentioned in the introduction, MR fluid is routinely modeled as a Bingham plastic. In typical applications, the damping from the passive component of the fluid is modeled as a constant. However, Lord Corporation’s web site revealed MR fluid’s viscosity increases at very low shear rates. These results are seen in this model. Figure 5.7 shows the relative velocity, which can be linearly linked to shear rate, and the viscosity of the fluid. As the relative velocity decreases, the viscosity of the fluid increases.

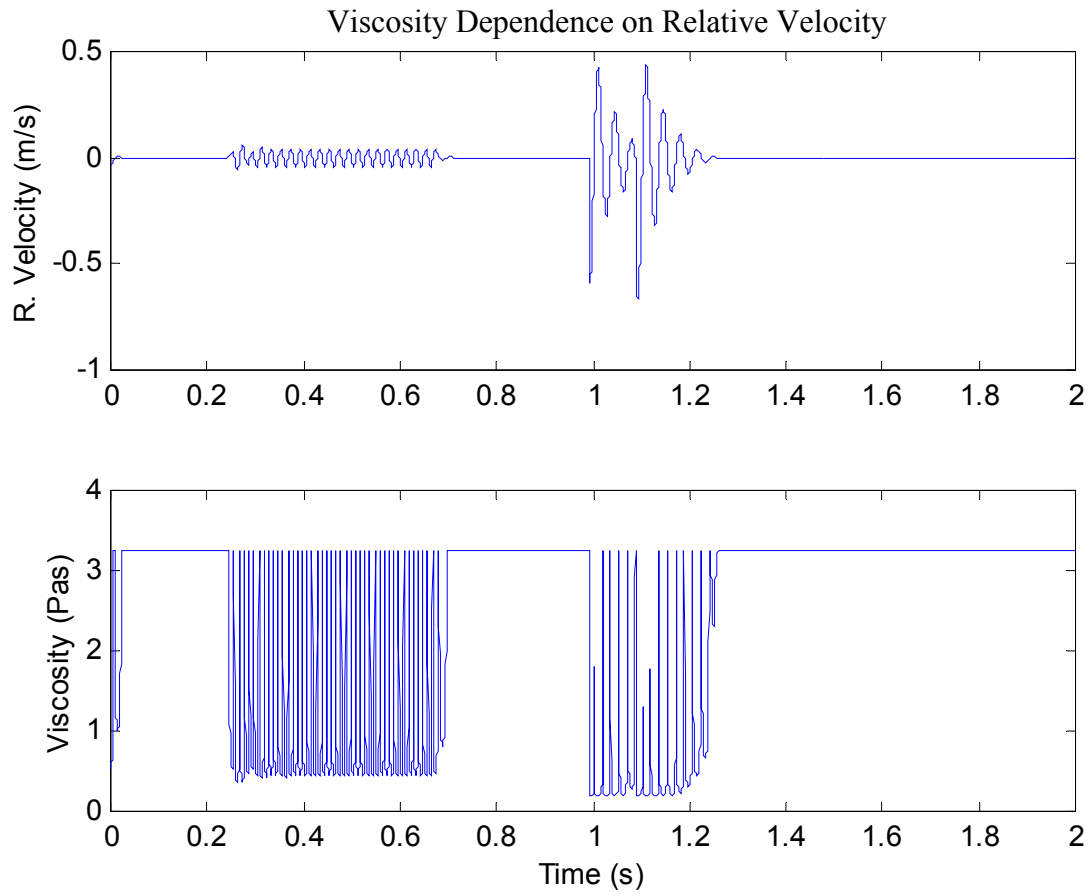


Figure 5.7. Viscosity is dependent on relative velocity.

CHAPTER 6. MR ISOLATOR COIL DESIGN

This chapter presents the detailed design of an isolator that can be used for the compressor application. The isolator could not be built within the scope of this thesis, but all the design information is presented to allow construction of the isolator. Building and testing the isolator is suggested as future work.

6.1 Determining the Necessary Yield Stress

Once the necessary yield stress needed for results is determined, the strength of the magnetic field needed to generate that yield stress is determined. Figure 6.1 shows the yield stress and magnetic flux results from the model.

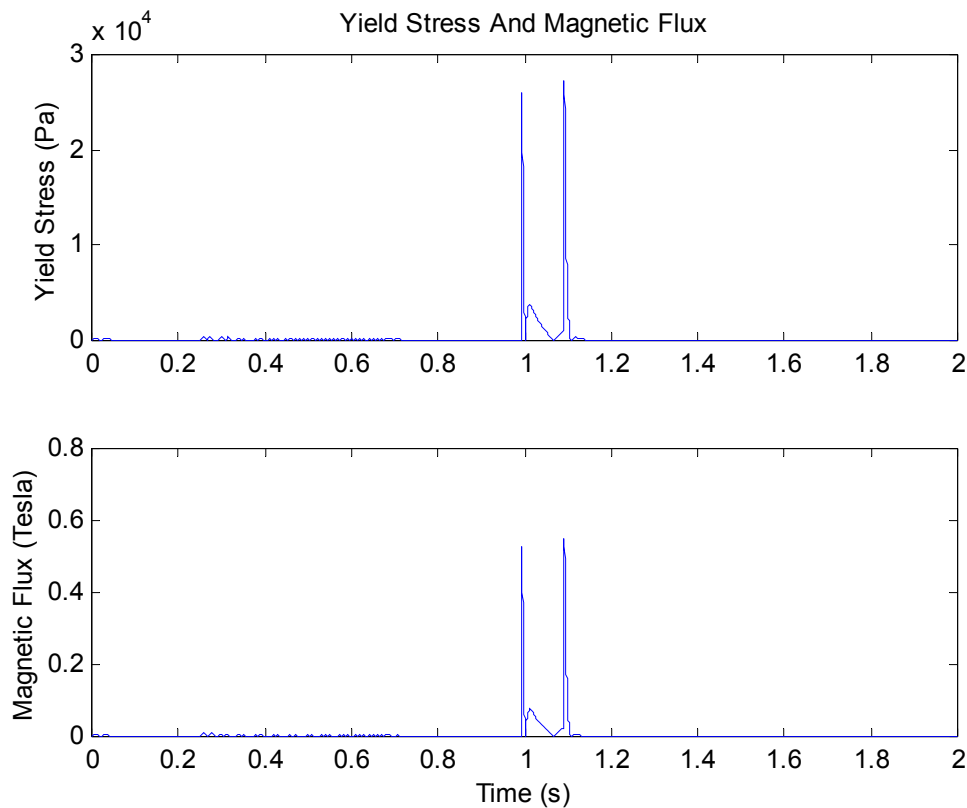


Figure 6.1. Yield stress and magnetic flux in model.

6.2 Electromagnetic Model of the Isolator

A finite element model of the isolator coil was developed in Quickfield, a software program designed to evaluate a system's electromagnetic properties [15]. Figure 6.2 shows the coil design that provided the flux necessary. Five hundred amp-turns were assumed for the coils.

This will be discussed later. The arrows indicate the intended flux pattern. Figure 6.3 shows the asymmetric model of the isolator. The magnetic flux levels in the isolator can be seen.

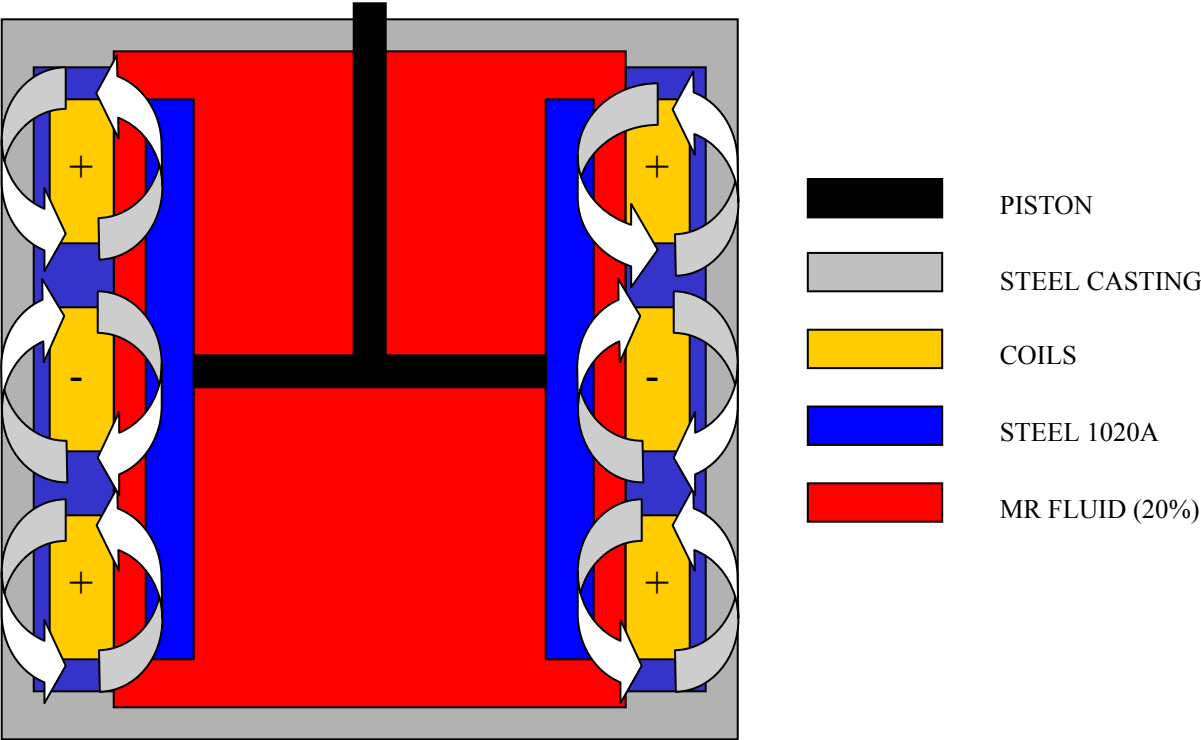


Figure 6.2. Coil design with intended flux pattern.

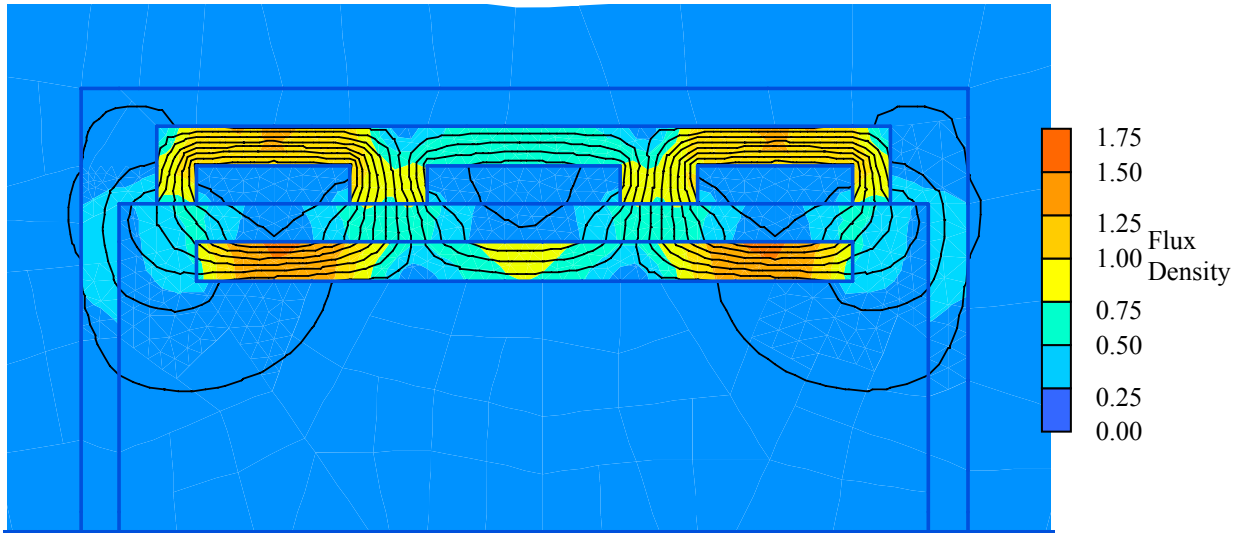


Figure 6.3. Finite element results showing flux in the isolator.

With the number of amp-turns and the area of the coils defined, the specifics of the coil, such as coil gage, coil length, voltage, and current, could be calculated. The equations used to calculate these parameters can be found in Appendix D. The analysis was run for different gage wires, and the results can be seen in the following figures. Again, these are the parameters required to get five hundred amp-turns.

6.3. Coil Properties

The following parameters were used in modeling the geometry of the coils. These parameters limit the area in which the coil can be wound. The equations used to determine the coil properties are found in Appendix D [16].

Coil Inner Diameter	17 mm
Coil Maximum Outer Diameter	19 mm
Coil Width	13 mm

Figure 6.4 shows the number of turns and coil mass as a function of wire gage. The number of turns is seen to jump from wire gage 24 to 25. When 25 gage wire is used, two layers of coils can fit in the area described above. With 24 gage wire, the wire is too thick to allow for a second layer of coils. This is why the number of turns is dramatically lower with 24 gage wire.

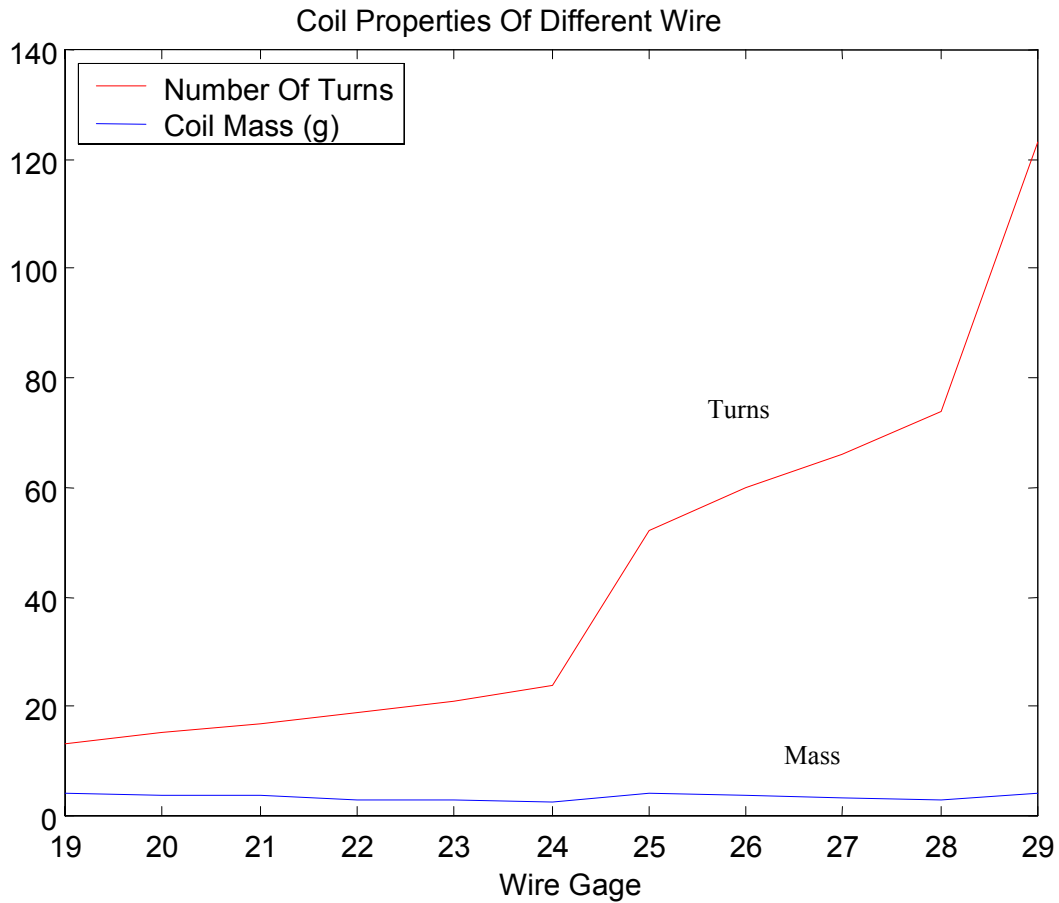


Figure 6.4. Number of coil turns and coil mass as a function of wire gage.

Figure 6.5 shows coil length and resistance as a function of wire gage. A large jump in coil length is seen between 24 and 25 gage wire. This can be attributed to the second layer of coils discussed above. When a second layer of coils becomes possible, considerably more wire is needed to make this second layer.

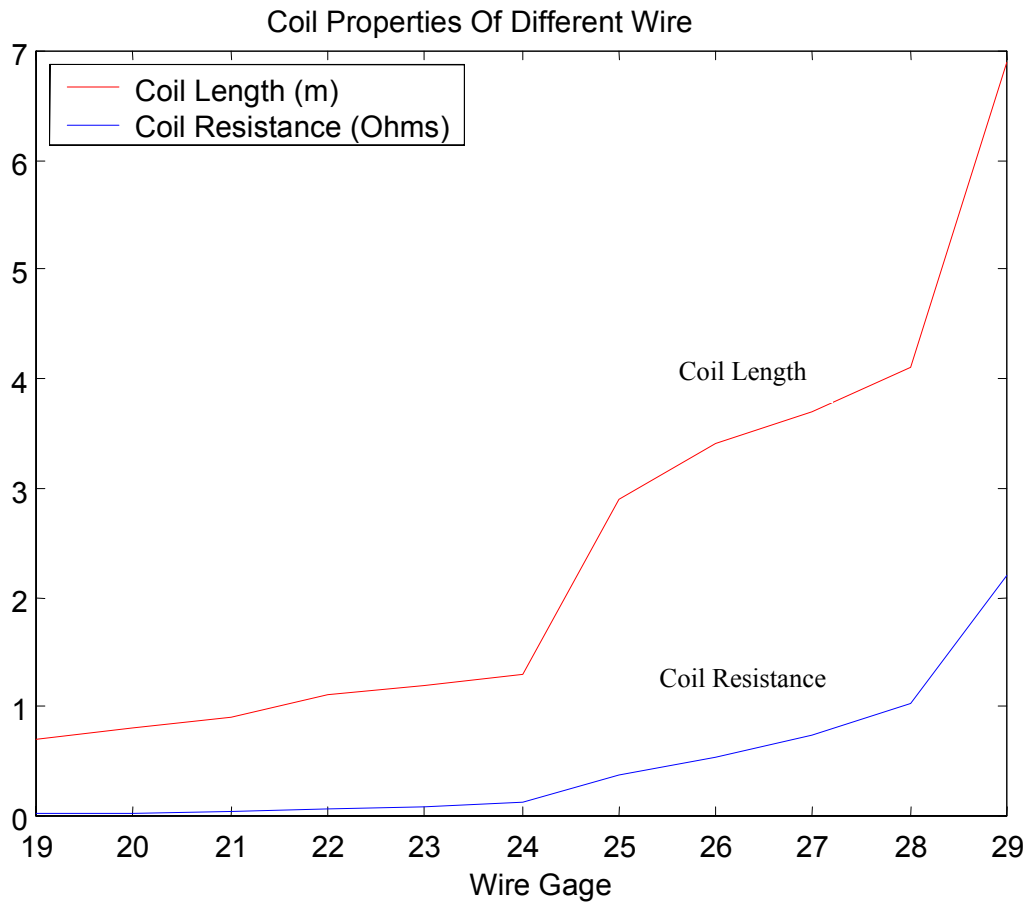


Figure 6.5. Coil length and resistance as a function of wire gage.

Personal discussions with design engineers for MR mounts revealed a well-designed coil will produce 500 amp turns. However, the efficiency of the coil begins to decrease when the coil is designed to produce more than 500 amp-turns [16]. Figure 6.6 shows the voltage and current in different gage wires needed to achieve 500 amp turns.

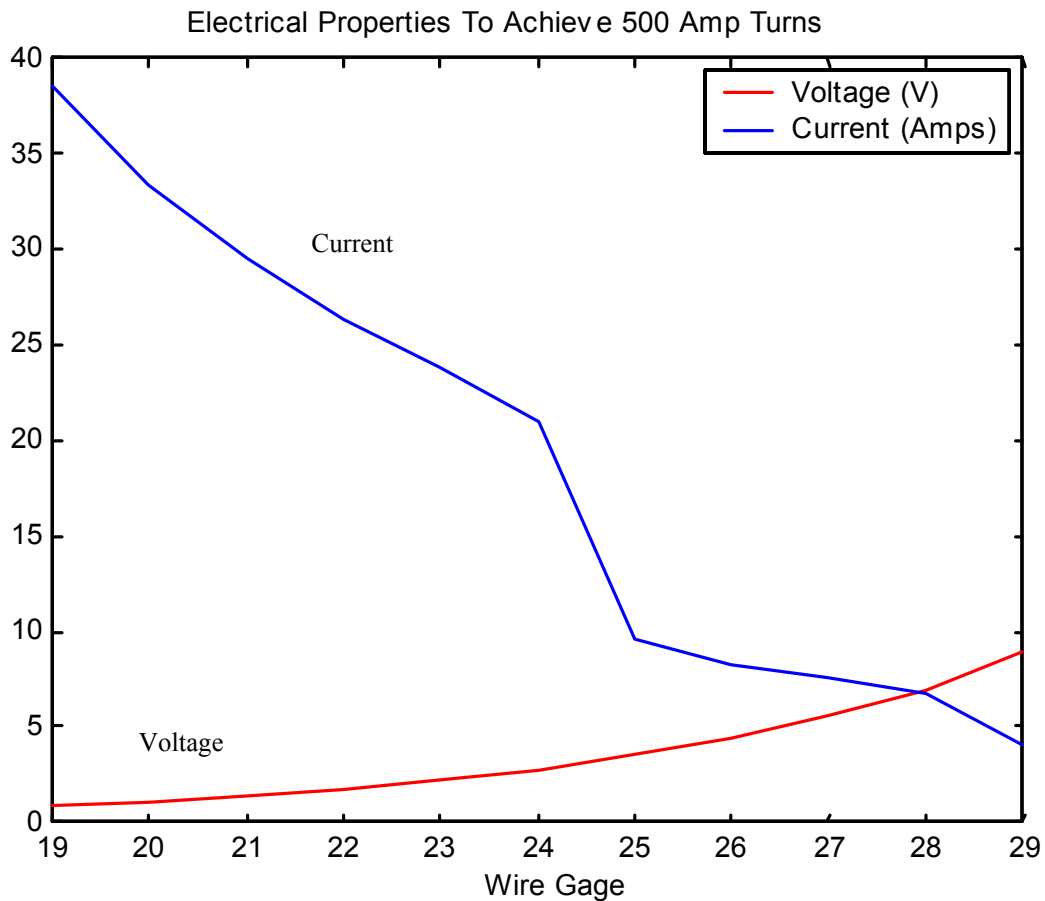


Figure 6.6. Voltage and current needed to achieve 500 amp turns.

The results show a tradeoff between coil length and current. With lower gage wire, the diameter of the wire is too large for the coils to be layered. This allows only a small coil length, and a large current is necessary to get the desired amp-turns. When higher gage wires are used, the coils are able to be layered. This is seen in the jump in number of coils and coil length between 24 gage and 25 gage wires. When the coils can be layered, the number of turns and wire length increase. The current, then, dramatically decreases. The voltage required increases as the wire gage increases.

6.4 Final Design

The final design of the optimal isolator can be seen below in Figure 6.7. Dimensions are in millimeters.

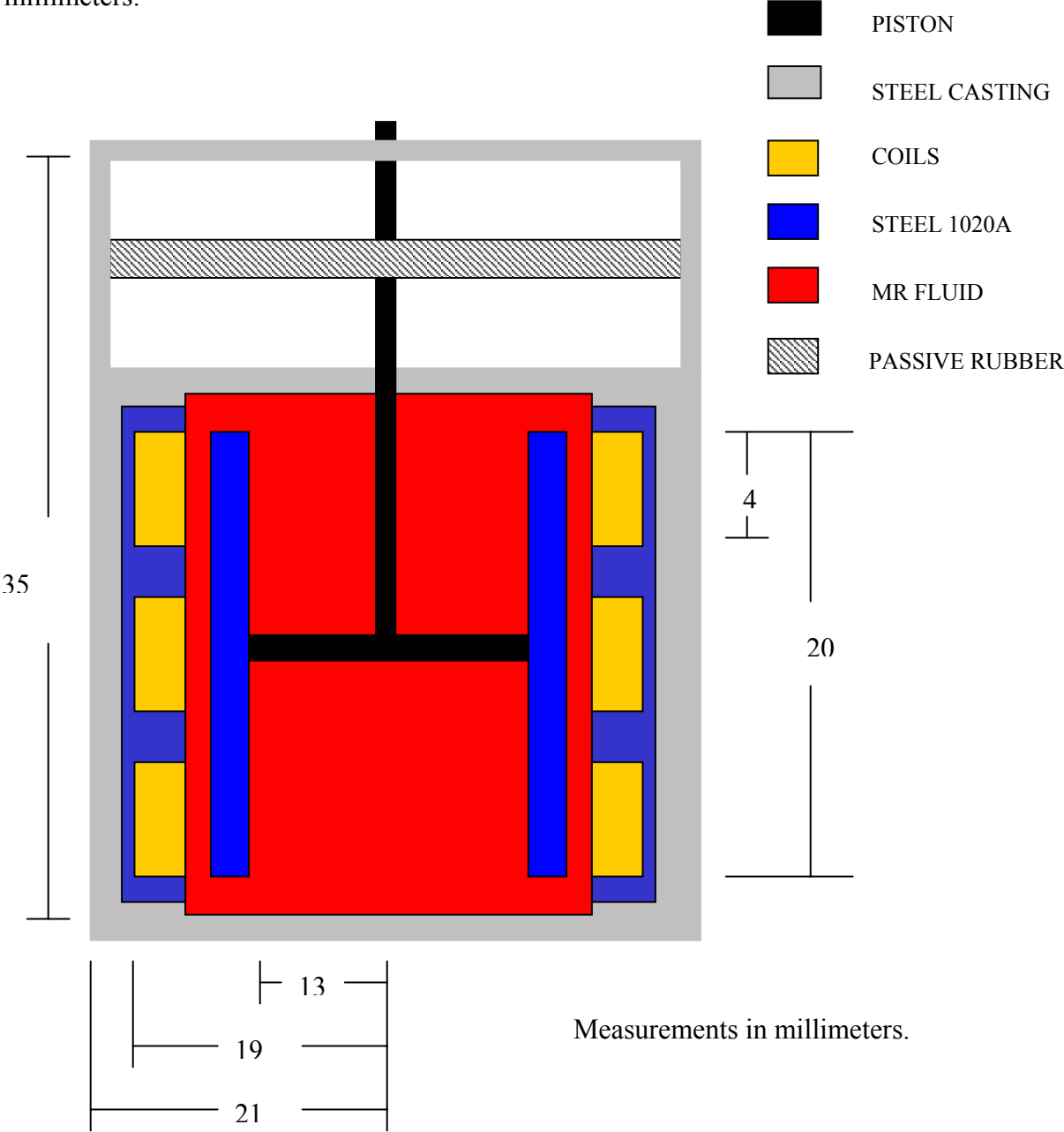


Figure 6.7. Proposed design of a MR based semi-active isolator.

Coil ID	17 mm		Plunger Diameter	13 mm
Coil OD	19 mm		Gap Width	1 mm
Coil Length	3.2 m		Channel Length	20 mm
Wire Gage	25		Fluid Volume	13 cc
Amps	10 A		Voltage	4 V

Table 6.1. Final design parameters.

The power requirements of the semi-active isolator increase as the relative velocity between the vehicle and the compressor increase. In this model, this occurs when the vehicle hits the bump. The isolator required maximum power of 0.7 W. This is seen in Figure 6.8. Since three isolators are needed for the isolation system, 2.1 W would be needed to power the three isolators, if they ran at optimal power. Loss factors would need to be factored in to determine the actual power requirements of the isolators.

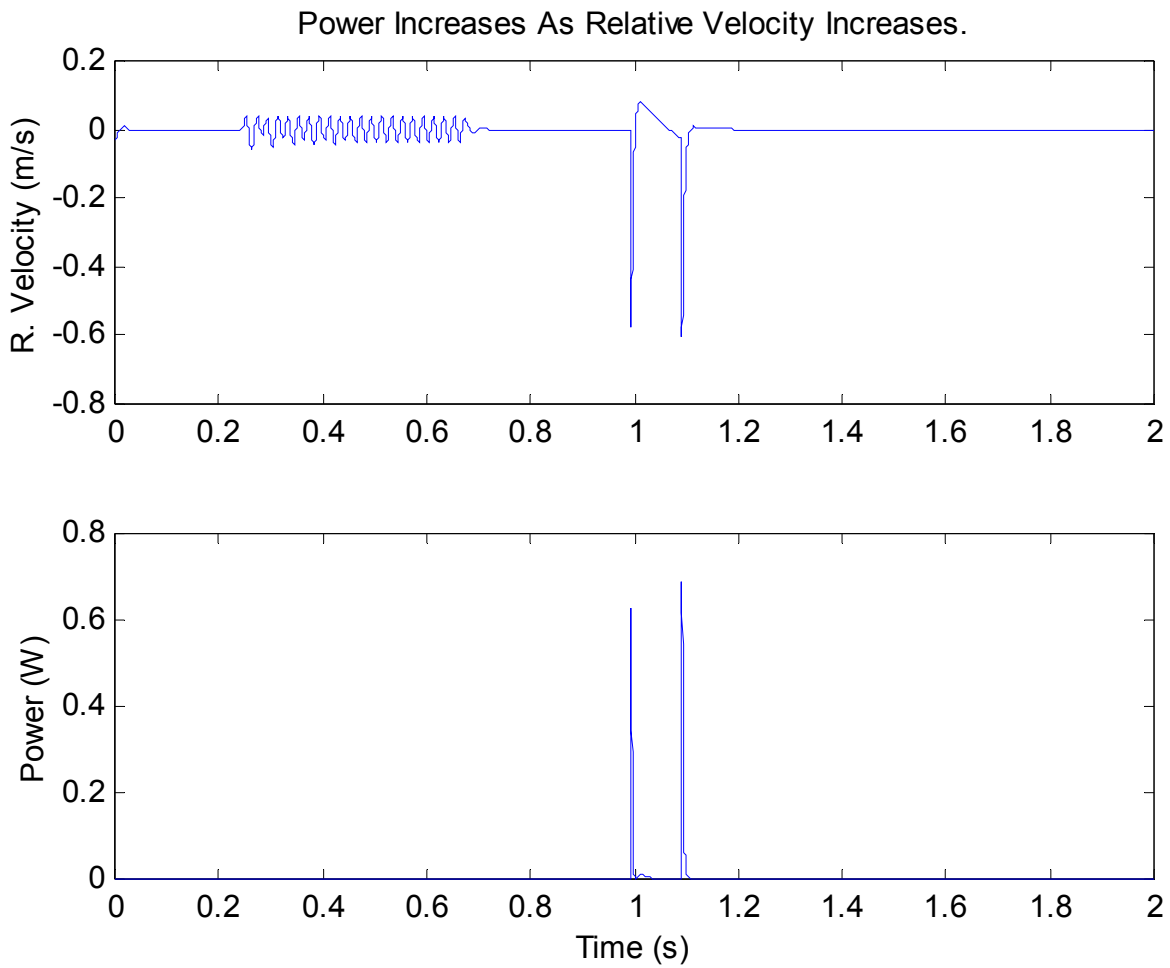


Figure 6.8. Power requirements of the semi-active isolator.

Table 6.2 calculates the overall weight of the isolator. The overall mass of the isolator comes to 238.2 grams, or 8.4 oz. This is significantly larger than the baseline isolator, which has a mass of 7.0 grams, or 0.25 oz. However, the isolator is still very light. Also, studies can be done to reduce mass, namely by replacing the steel with a lighter weight material.

Component	Density	Volume	Mass (g)
Rubber and Piston	_____	_____	7.3 ⁽¹⁾
MR Fluid	3.005 g/cc	13 cc	39.1
Coils	_____	_____	4 ⁽²⁾
Steel Casting	7900 kg/m ³	1.71E-5 m ³	135.1
Flux Guide (Steel)	7900 kg/m ³	6.67E-6 m ³	52.7
Total	_____	_____	238.2

Notes: (1) Weighed sample parts, (2) From Figure 6.4.

Table 6.2. Mass of the semi-active isolator.

CHAPTER 7. CONCLUSIONS

This thesis has investigated many aspects of the design of a semi-active MR isolator for an automotive application. The final isolator design proposed reduces the high frequency vibration transmitted from the compressor to the automobile, and also limits the relative vibration of the compressor due to vehicle road inputs. This performance was not able to be achieved using a passive isolator. The isolator slightly increases the weight of the compressor and mount, and it adds some complexity to the automobile. The isolator requires very minimal power to operate. The durability of the mechanical components and of the proposed sensor in the isolator is expected to be high due to the simple design. A detailed summary of what has been learned from this investigation is given below.

7.1 Comments

The following characteristics are considered optimal based on the research conducted

- In the optimal design produced, a soft rubber mount is used in parallel with the MR isolator. The rubber mount is necessary for the static stability of the isolator. Without this component, the MR isolator will naturally ground out due to the weight of the compressor. The rubber component needs to be very soft to reduce the transmitted noise. However, if the rubber component is made too soft, the isolator will not be able to meet baseline performance regardless of how efficient the active component of the MR fluid is.
- The isolator should be designed to make the MR fluid work in the flow mode. This mode is the simplest to design, while providing the necessary damping force to get results.

- A MR fluid with low viscosity and high yield stress is desired. Use of the MR fluid is more efficient if the active component is much larger than the passive component. A low viscosity will decrease the passive resistance, while a large yield stress allows the active component to increase.
- The control method developed scales the active component of the MR fluid based on the relative velocity. A skyhook algorithm does not allow the MR fluid's active component to always react at the correct time.
- Low pass filter capabilities need to improve. When a Butterworth low pass filter was used, the semi-active isolator showed an improvement of 55%. However, when the filter was turned off, an improvement of 83% was seen.
- A small coil design was able to generate the necessary magnetic field in the MR fluid.
- A wire gage of 25 was found to be optimal. Anything larger than this limits the number of turns available and, therefore, dramatically increases the amount of current needed. While going with a gage of 25 requires more wire length to get the necessary field, it negates the concern of a thermal event due to extremely high current.
- The semi-active isolator has significantly more mass than the baseline isolator. However, the semi-isolator is still light and feasible for use in automotive applications. The substitution of lighter materials would reduce the weight of the isolator.

CHAPTER 8. RECOMMENDATIONS FOR FUTURE WORK

This chapter discusses some research items that should be investigated in the future to improve the performance and complete the development of this semi-active isolator.

8.1 Items for Future Research

- (i) A control algorithm based on minimizing the transmitted force and minimizing the relative displacement may improve the performance of the isolator. However, this would increase the complexity of the control system and hardware. Bang-bang control possibly based on the relative displacement of the compressor could also be investigated as a simple control approach.
- (ii) The filter used with the control algorithm needs to be improved. The problems resulting from phase lag were quite apparent. While an ideal filter may never be possible, development of a filter that minimizes phase lag would dramatically improve results when the filter is on.
- (iii) A fluid that has low viscosity and a high shear stress is ideal. High viscosity hinders the transmissibility performance of the isolator, and low shear stresses do not allow the active component of the MR fluid to be effective.
- (iv) Further optimization of the coil design would allow the isolator to more effectively use the unique capabilities of the MR fluid and perhaps be reduced in size.
- (v) Building and testing of a prototype isolator is needed to validate the performance described in this thesis.

- (vi) Cost and weight improvement studies will need to be conducted once the performance of the isolator is validated.
- (vii) The variation in the rubber stiffness and damping with temperature should be investigated in the final design. Also, the variation in fluid viscosity and the change in MR performance with temperature should be investigated.
- (viii) A bi-linear rubber isolator could also be investigated as a compromise between the linear passive and semi-active designs or for use with the semi-active design.

BIBLIOGRAPHY

- [1] Karnopp, Dean, and Margolis, Donald, "Adaptive Suspension Concepts for Road Vehicles," *Vehicle System Dynamics*, Vol. 13 (1984), pp. 145-160.
- [2] Hutton, David V., *Applied Mechanical Vibrations*, McGraw Hill Publishing, New York, 1981.
- [3] Srinivasan, A. V. and McFarland, D. Michael, *Smart Structures, Analysis and Design*, Cambridge University Press, New York, 2001.
- [4] Spencer Jr, B. F., Dyke, S. J., Sain, M. K., and Carlson, J. D., "Phenomenological Model of a Magnetorheological Damper," *ASCE Journal of Engineering Mechanics*, March 10, 1996.
- [5] Jolly, Mark R., Bender, Jonathan W., and Carlson, J. David. "Properties and Applications of Commercial Magnetorheological Fluids. SPIE Vol. 3327, pp. 262-275.
- [6] Pang, Li, Kamath, Gopalakrishna M., Wereley, Norman M., "Dynamic Characterization and Analysis of Magnetorheological Damper Behavior," SPIE Vol. 3327, pp. 284-302.
- [7] Tewani, Sanjiv. *Advanced Mounts and Suspensions Supervisor*. Delphi Corporation. Personal discussion. February, 5, 2002.
- [8] Bolter, Ralf, and Janocha, Hartmut, "Design Rules for MR Fluid Actuators in Different Working Modes," SPIE Vol. 3045, pp. 148-159.
- [9] Sproston, J. L., and el Wahed, A. K. , "A Comparison of the Performance of ER Fluids in Squeeze," *Proceedings of the 5th International Conference on Electrorheological Fluids, Magnetorheological Suspensions and Associated Technology*, Sheffield, UK, July 10-14, pp. 259-269.
- [10] www.rheonetic.com, Lord Corporation..
- [11] Bathe, K.-J. and Wilson, E. L., *Numerical Methods in Finite Element Analysis*, Prentice-Hall, Inc., Englewood Cliffs, NJ, 1976..
- [12] MATLAB SPTOOL. MATLAB Version 5.3. The Math Works Inc.
- [13] Soong, T. T., *Active Structural Control: Theory and Practice*, Longman Scientific and Technical, New York, 1990.
- [14] <http://www.rdpe.com/displacement/lvdt/lvdt-principles.htm>, RDP Group.

- [15] Quickfield 4.3. Tera Analysis Ltd. 2002.
- [16] Hopkins, Patrick. MR Mount Engineer. Delphi Corporation. Personal discussion. April, 18, 2002.
- [17] Bolter, Ralf, and Janocha, Hartmut, "Performance of Long Stroke and Low Stroke MR Fluid Damper," SPIE Vol. 3327, pp. 303-313.
- [18] Firoozian, R., "A Non-Linear Model for Dynamic Response of Electrorheological Fluid in Flow Mode," Proceedings of the 5th International Conference on Electrorheological Fluids, Magnetorheological Suspensions and Associated Technology, Sheffield, UK, July 10-14, pp. 291-299.
- [19] Janocha, H., Rech, B., and Bolter, R., "Practice-Relevant Aspects of Constructing ER Fluid Actuators," Proceedings of the 5th International Conference on Electrorheological Fluids, Magnetorheological Suspensions and Associated Technology, Sheffield, UK, July 10-14, pp. 435-447.
- [20] Jeon, D., Park, C., and Park, K., "Vibration Suppression by Controlling an MR Damper," Proceedings of the 6th International Conference on Electrorheological Fluids, Magnetorheological Suspensions and Their Applications, Yonezawa, Japan, July 22-25, pp. 853-860.
- [21] Jeon, Y. S., Choi, Y. T., Choi, S. B., and Cheong, C. C., "Performance Evaluation of a Mixed Mode ER Engine Mount via HILS," Proceedings of the 7th International Conference on Electrorheological Fluids and Magnetorheological Suspensions, Honolulu, Hawaii, July 19-23, pp. 812-820.
- [22] Khusid, B, Acrivos, A., Khodorkovsky, and Beltran, M., "Electrorheological Squeeze-Flow Shock Absorber," Proceedings of the 6th International Conference on Electrorheological Fluids, Magnetorheological Suspensions and Their Applications, Yonezawa, Japan, July 22-25, pp. 705-712.
- [23] Kim, K., Lee, J., and Jeon, D., "Vibration Suppression of an MR Fluid Damper System with Frequency Shaped LQ Control," Proceedings of the 7th International Conference on Electrorheological Fluids and Magnetorheological Suspensions, Honolulu, Hawaii, July 19-23, pp. 648-656.
- [24] Lee, H. G., Choi, S. B., Han, S. S., Kim, J. H., and Suh, M. S., "Bingham and Response Characteristics of ER Fluids in Shear and Flow Modes," Proceedings of the 7th International Conference on Electrorheological Fluids and Magnetorheological Suspensions, Honolulu, Hawaii, July 19-23, pp. 523-530.

- [25] Leek, T. H., Lingard, S., Bullough, W. A., and Atkin, R. J., "The Time Response of an Electro-rheological Fluid in a Hydrodynamic Film," Proceedings of the 5th International Conference on Electrorheological Fluids, Magnetorheological Suspensions and Associated Technology, Sheffield, UK, July 10-14, pp. 551-563.
- [26] Li, W. H., Wang, X. J., Tang, X., and Zhang, P. Q., "Generalized Analysis of Channel Flow of ER/MR Fluids Through Complex Geometries," Proceedings of the 6th International Conference on Electrorheological Fluids, Magnetorheological Suspensions and Their Applications, Yonezawa, Japan, July 22-25, pp. 347-355.
- [27] Mui, G., Russell, D. L., and Wong, J. Y., "Non-Linear Parameter Identification of an Electro-Rheological Fluid Damper," Proceedings of the 5th International Conference on Electrorheological Fluids, Magnetorheological Suspensions and Associated Technology, Sheffield, UK, July 10-14, pp. 690-697.
- [28] Riha, P., Kimura, H., Takimoto, J., and Koyama, K., "Stochastic Aspects of Bridging Bonds of Induced Structure of Electrorheological Fluids in Shear Flow," Proceedings of the 6th International Conference on Electrorheological Fluids, Magnetorheological Suspensions and Their Applications, Yonezawa, Japan, July 22-25, pp. 156-163.
- [29] See, H., Sakurai, R., and Saito, T., "Model of Structure and Conduction in an Electrorheological Fluid under Flow," Proceedings of the 5th International Conference on Electrorheological Fluids, Magnetorheological Suspensions and Associated Technology, Sheffield, UK, July 10-14, pp. 478-485.
- [30] Shimada, K. et al, "Rheology of ERF on Various Flow Fields," Proceedings of the 6th International Conference on Electrorheological Fluids, Magnetorheological Suspensions and Their Applications, Yonezawa, Japan, July 22-25, pp. 256-262.
- [31] Sproston, J. L., el Wahed, A. K., and Stanway, R., "Electrorheological Fluids in Squeeze under AC and DC Excitation," Proceedings of the 6th International Conference on Electrorheological Fluids, Magnetorheological Suspensions and Their Applications, Yonezawa, Japan, July 22-25, pp. 223-231.
- [32] Tang, X., Li, W. H., Wang, X. J., and Zhang, P. Q., "Testing and Modeling of an MR Damper in the Squeeze Flow Mode," Proceedings of the 6th International Conference on Electrorheological Fluids, Magnetorheological Suspensions and Their Applications, Yonezawa, Japan, July 22-25, pp. 870-886.
- [33] Tang, X., Li, W. H., Wang, X. J., and Zhang, P. Q., "Structure Evolution of Electrorheological Fluids under Flow Conditions," Proceedings of the 6th International Conference on Electrorheological Fluids, Magnetorheological Suspensions and Their Applications, Yonezawa, Japan, July 22-25, pp. 164-171.

- [34] Tao, R., Zhang, J., Shiroyanagi, Y., Tang, X., and Zhang, X., "Electrorheological Fluids Under Shear," Proceedings of the 7th International Conference on Electrorheological Fluids and Magnetorheological Suspensions, Honolulu, Hawaii, July 19-23, pp. 411-422.
- [35] Yamamoto, H. and Nakano, M., "Dynamic Viscoelasticity and Its Mechanical Model of an MR Suspension in Oscillatory Slit Flow Mode," Proceedings of the 7th International Conference on Electrorheological Fluids and Magnetorheological Suspensions, Honolulu, Hawaii, July 19-23, pp. 665-673.
- [36] Wang, X., Zhang, P. Q., Tang, X., and Tao, R., "Testing and Modeling a Cone-Shaped Squeeze-Film Mode," Proceedings of the 7th International Conference on Electrorheological Fluids and Magnetorheological Suspensions, Honolulu, Hawaii, July 19-23, pp. 804-811.
- [37] Weyenberg, T. R., Piolet, J. W., and Petek, N. K., "The Development of Electrorheological Fluids for an Automotive Semi-Active Suspension System," Proceedings of the 5th International Conference on Electrorheological Fluids, Magnetorheological Suspensions and Associated Technology, Sheffield, UK, July 10-14, pp. 395-403.

APPENDIX A

- Computer algorithm to compute transmissibility of a passive isolator.

```

clear all
clc

k=[10000 30000 50000];           % Stiffness in N/m
m=1;                             % Mass in kg
zeta=.1;                          % Damping Ratio
c=zeta.*(2*sqrt(k.*m));          % Damping coefficient in N*s/m
freq=0:0.25:401;                 % Frequency range
w=freq.*2*pi;                    % Conversion to radians
ratio=freq./((sqrt(k(3)/m))/(2*pi)); % w/wn

% Developing transfer path
for x=1:3
    for i=1:1605
        AA(x,i)=(abs(k(x)+j*c(x)*w(i))
                ./((abs(k(x)+j*c(x)*w(i)-m*w(i)^2))); % Trans. Equation
    end
end

% Plotting transfer paths

figure(1)
subplot(3,1,1), plot(freq,AA(1,1:1605),'k')
title('Transfer Path As Function Of Frequency')
ylabel('X/Y'), legend('k=16000 c=70 m=1 zeta=0.2767')
axis([0 300 0 3])
subplot(3,1,2), plot(freq,AA(2,1:1605),'r')
ylabel('X/Y'), legend('k=16000 c=140 m=1 zeta=0.5534')
axis([0 300 0 3])
subplot(3,1,3), plot(freq,AA(3,1:1605),'b'), xlabel('Frequency')
ylabel('X/Y'), legend('k=16000 c=210 m=1 zeta=0.8301')
axis([0 300 0 3])

figure(2)
semilogy(ratio,AA(1,1:1605),'k'),hold,plot(ratio,AA(2,1:1605),'r')
plot(ratio,AA(3,1:1605),'b')
legend('k=10000 N/m','k=30000 N/m','k=50000 N/m'),axis([0 10 .01 10])
xlabel('w/wn'), ylabel('X/Y')
title('Transmissibility As Function Of Frequency Ratio'), hold

```

APPENDIX B

- Computer algorithm for the single degree of freedom passive model.

```

clear all      % Passive Model
clc           % Greg Stelzer, Thesis Code

% Integration Variables
xr=0; vr=0; ar=0; acce=0;
maxtime=2; samplerate=1*4096;
points=maxtime*samplerate; dt=1/samplerate;
t=linspace(0,maxtime,points);

% Road Surface Variables
freq1=1; omega1=2*pi*freq1; a=.00508; % Frequency and amplitude of body
freq2=5; omega2=2*pi*freq2; aa=.01905; % Frequency and amplitude of bump
y=a*sin(omega1*t); % Road displacement
y(4073:4472)=a*sin(omega1*t(4073:4472)) % as a function
+aa*sin(omega2*t(1:400)); % of time
ydot=a*omega1*cos(omega1*t); % Road velocity
ydot(4073:4472)=a*omega1*cos(omega1*t(4073:4472)) % as a function
+aa*omega2*cos(omega2*t(1:400)); % of time

% Compressor Variables
freqc=50; b=10; m=1; % Speed and amplitude of compressor force, compressor mass
Fcomp(1:points)=0; % Forcing function generated
Fcomp(1000:2750)=b*sin(2*pi*freqc*t(1:1751)); % by the compressor

% Isolation Variables
k=50000; % Passive stiffness provided by rubber
c=.1*2*sqrt(k*m); % Passive damping provided by rubber

for i=1:points
    for iter=1:10
        displ=xr+vr*dt+(.25*ar+.25*acce)*dt*dt; % Numerically integrate for displacement
        vel=vr+(.5*ar+.5*acce)*dt; % Numerically integrate for velocity
        acce=(1/m)*(k*(-displ+y(i))+c*(-vel+ydot(i))+Fcomp(i)); % Equation of motion
    end
    xr=displ; vr=vel; ar=acce; % Reset
    displacement(i)=displ; % values
    velocity(i)=vel; % for next
    acceleration(i)=acce; % time step
end

transmitted=k*(displacement(1000:2750)-y(1000:2750))+c*(velocity(1000:2750)-ydot(1000:2750)); %
    Transmitted force during NS run

% FFT Of Transmitted Force
N=samplerate; n=length(transmitted)/N;
q=zeros(1,N-length(transmitted));

```

```

transmitted=[transmitted,q];
disp([' Time history padded with ',int2str(length(q)), ' zeros'])
n=length(transmitted)/N;

for k=1:2*n-1 q=(k-1)*(N/2)+1; Xm(k,:)=transmitted(q:(q+N-1)); end
[M,N]=size(Xm); avgs=M; twin=hanning(N); gain = 0.5; BW = 1.5; twin=twin'/gain;
for k=1:M Xm(k,:)=Xm(k,:).*twin; end
Xm=fft(Xm');
for k=1:M Xm(k,:)=Xm(k,:).*conj(Xm(k,:))/N^2; end
Xm=Xm(:,1:(N/2+1));
for k=1:M Xm(k,2:N/2)=2*Xm(k,2:N/2); end
if M ~= 1 Pxx=mean(Xm); else Pxx=Xm; end
deltaf=samplerate/N; freq=linspace(0,N/2,N/2+1)*deltaf;
%Pxx=sqrt(Pxx);

reldispl=displacement-y; % Calculates relative displacement in passive system
relvel=velocity-ydot; % Calculates relative velocity in passive system
transmitted=k*(displacement-y)+c*(velocity-ydot);% Transmitted force during run

% Absolute Amplitudes Plot
figure(1)
subplot(3,1,1), plot(t,displacement), axis([0 maxtime -2.5e-2 2.5e-2])
title('Passive Isolator'), ylabel('DISPLACEMENT')
subplot(3,1,2), plot(t,velocity), axis([0 maxtime -1.25 1.25]), ylabel('VELOCITY')
subplot(3,1,3), plot(t,acceleration), axis([0 maxtime -150 150]), ylabel('ACCELERATION')

% Isolator Results
figure(2)
%subplot(3,1,1), plot(t(1000:5095),transmitted), axis([0 maxtime -20 20]), title('Passive Isolator'),
ylabel('TRANSMITTED FORCE')
subplot(3,1,2), plot(t,reldispl), axis([0 maxtime -2.5e-3 2.5e-3])
ylabel('RELATIVE DISPLACEMENT')
subplot(3,1,3), semilogy(freq,Pxx), axis([0 512 10^-4 10])
ylabel('PS Of Transmitted Force')

figure(3)
subplot(4,1,1),plot(t,y), axis([0 2 -.05 .05]), ylabel('Body Movement (m)')
title('Passive Model Results -- wn=35.8 Hz, zeta=0.1')
subplot(4,1,2),plot(t,reldispl), axis([0 2 -3e-3 3e-3]), ylabel('Rel. Disp. (m)')
subplot(4,1,3),plot(t,transmitted), axis([0 2 -30 30])
ylabel('Transmitted Force (N)'), xlabel('Time (s)')
subplot(4,1,4),semilogy(freq,Pxx), axis([0 200 10e-6 10])
ylabel('PS @ 50 Hz (N^2/Hz)')

```

```
maxreldispl=max(abs(reldispl)) % Display maximum relative displacement  
comptrans=Pxx(51) % Display NS portion of the PS of the transmitted noise
```

APPENDIX C

- Computer algorithm for the single degree of freedom semi-active model.

```

clear all % Isolation Improvement Model
clc      % Greg Stelzer, Thesis Code

% Integration Variables
xr=0; vr=0; ar=0; acce=0;
maxtime=2; samplerate=1*4096;
points=maxtime*samplerate; dt=1/samplerate;
t=linspace(0,maxtime,points);

% Road Surface Variables
freq1=1; omega1=2*pi*freq1; a=.00508;% Frequency and amplitude of body
freq2=5; omega2=2*pi*freq2; aa=.01905;% Frequency and amplitude of bump
y=a*sin(omega1*t); % Road displacement as a
y(4073:4472)=a*sin(omega1*t(4073:4472))+aa*sin(omega2*t(1:400));% function of time
ydot=a*omega1*cos(omega1*t); % Road velocity
ydot(4073:4472)=a*omega1*cos(omega1*t(4073:4472))+aa*omega2*cos(omega2*t(1:400));

% Compressor Variables
freqc=50; b=10; m=1;%Speed and amplitude of compressor force, compressor mass
Fcomp(1:points)=0; Fcomp(1000:2750)=b*sin(2*pi*freqc*t(1:1751)); % Forcing function
generated by the component

% Isolation Variables
k=30000; % Passive stiffness provided by rubber
c=.1*2*sqrt(k*m); % Passive damping provided by rubber

% Fluid Properties -- MRF 132LD
srf=[0 2.5 5 7.5 10 15 20 40 60 80 100 120 140 10000]; % Shear rate
visc=[3.25 3.25 2 1.3 1.15 .8 .65 .45 .35 .3 .25 .225 .2 .2]; % Viscosity as a function of shear
rate with no magnetic field
Hf=[0 50 100 150 200 250 300]*1000; % Magnetic induction
ysf=[0 14.8 27 36.5 41 44 45]*1000; % Yield stress as a function of magnetic induction
Bf=[0 .3 .55 .65 .75 .8 .85]; % Magnetic Flux
density=3005.5; % Density of fluid (3.0055 g/cc)

% Filter Properties
[C,A]=butter(2,(15*2)/samplerate); % Second Order Butterworth Low Pass Filter Properties
load butterworth_2
figure(1)
subplot(2,1,1), plot(filt1.f,abs(filt1.H)),title('Second Order Butterworth Low Pass Filter
Properties -- 30 Hz')
xlabel('Frequency (Hz)'), ylabel('Magnitude'), axis([0 200 0 1])
subplot(2,1,2), plot(filt1.f,angle(filt1.H)*180./pi)
xlabel('Frequency (Hz)'), ylabel('Phase (deg)'), axis([0 200 -200 0])

% Geometry Properties

```

```

ri=.013; h=.001; ro=ri+h; b=pi*(ri+ro); L=.020; % Inner radius, gap, outer
radius, coil length, average circumference
Ai=pi*ri^2; Ao=pi*ro^2; Agap=Ao-Ai; volume=(pi*ro^2)*L % Inner area, outer area,
gap area, fluid volume
F=Agap; II=2*pi*(ro+ri); Dh=4*F/II; % Values used to
X1=ro^4-ri^4; X2=(ro^2-ri^2)^2; X3=log(ro/ri); % calculate Reynolds number

for i=1:points
for iter=1:10
displ=xr+vr*dt+(.25*ar+.25*acce)*dt*dt; % Numerically Integrate For Displacement
vel=vr+(.5*ar+.5*acce)*dt; % Numerically Integrate For Velocity
reldispl(i)=displ-y(i); % Calculate Relative Displacement
relvel(i)=vel-ydot(i); % Calculate Relative Velocity

sr(i)=relvel(i)/h; % Calculate Shear Rate
j=2; % Interpolation Counter
while abs(sr(i))>srf(j) % Linear Interpolation
j=j+1; % To Calculate
end % Viscosity From
viscosity(i)=visc(j)-(((srf(j)-abs(sr(i)))/(srf(j)-srf(j-1))))*(visc(j)-visc(j-1))); % Shear Rate
Re(i)=(relvel(i)*Dh)/(viscosity(i)/density); % Calculation Of Reynold's Number
Q(i)=relvel(i)*Ai; % Calculation Of Flow

w(i)=relvel(i);
%if vel*(vel-ydot(i))>0 %
%w(i)=relvel(i); % Skyhook
%else % Control
%w(i)=0; %
%end %

%if i>=4001 %
% z(i)=v(i); % Perfect Filter
%elseif i>=3 & i<=4000 %
if i>=3
z(i)=C(1)*v(i)+C(2)*v(i-1)+C(3)*v(i-2)-A(2)*z(i-1)-A(3)*z(i-2);%
elseif i==2 % Lowpass
z(i)=C(1)*v(i)+C(2)*v(i-1)+A(2)*z(i-1); % Filter
else %
z(i)=C(1)*v(i); %
end %

scale=5000; % Scale Factor For Yield Stress
ys(i)=z(i)*scale; % Setting yield stress equal to scaled relative velocity, after skyhook
control and lowpass filter

```

```

T(i)=(b*h^2*ys(i))/(12*Q(i)*viscosity(i)); % Flow Characteristic Value From Smart
Structures Book
mrforce_ss(i)=Agap*((3*L*ys(i))/h); % Semi-active MR Force From Smart
Structures Book
%mrforce_fm(i)=Agap*((2*L*ys(i))/h); % Semi-active MR Force From Fluid
Mechanics Book
fyield(i)=mrforce_ss(i); % Worst Case fyield Term
cmr_ss(i)=Agap*Ai*((12*viscosity(i)*L)/(b*(h^3))); % MR Fluid Passive Damping
From Smart Structures Book
%cmr_fm(i)=Agap*Ai*(8*viscosity(i)*L)/(pi*(X1-(X2/X3)))-
(Agap*density*9.81*L)/abs(relvel(i)); % MR Fluid Passive Damping From Fluid Mechanics
Book
cmr(i)=cmr_ss(i); % Worst Case MR Fluid Passive
Damping
pressure(i)=((2*L*ys(i))/h)+((12*Q(i)*viscosity(i)*L)/(b*(h^3))); % Pressure Difference In
Fluid

acce=(1/m)*(k*(-displ+y(i))+(c+cmr(i))*(-vel+ydot(i))-fyield(i)+Fcomp(i)); % Equation
Of Motion
end
xr=displ; vr=vel; ar=acce; % Reset
displacement(i)=displ; % Values
velocity(i)=vel; % For Next
acceleration(i)=acce; % Time Step

j=2; % Interpolation Counter
while abs(ys(i))>ysf(j) % Linear Interpolation
    j=j+1; % Interpolation
end % To Calculate
H(i)=Hf(j)-(((ysf(j)-abs(ys(i)))/(ysf(j)-ysf(j-1)))*(Hf(j)-Hf(j-1))); % Magnetic Inductance
From Yield Stress
B(i)=Bf(j)-(((ysf(j)-abs(ys(i)))/(ysf(j)-ysf(j-1)))*(Bf(j)-Bf(j-1))); % Magnetic Flux From
Yield Stress
power(i)=volume*B(i)*H(i); % Power Required
end

transmitted=k*(displacement(1000:2750)-
y(1000:2750))+(c+cmr(1000:2750)).*(velocity(1000:2750)-
ydot(1000:2750))+fyield(1000:2750); % Transmitted Force
spring=k*(displacement-y); % Passive Spring Force
damper=c*(velocity-ydot); % Passive Damping Force
cmrforce=cmr.*(velocity-ydot); % Passive MR Fluid Damping Force
mryieldforce=fyield; % Semi-active MR Fluid Damping Force
mrforce=cmr.*(velocity-ydot)+fyield; % Total MR Fluid Damping Force

% FFT Of Transmitted Force

```

```

N=samplerate; n=length(transmitted)/N;
q=zeros(1,N-length(transmitted));
transmitted=[transmitted,q];
disp([' Time history padded with ',int2str(length(q)), ' zeros'])
n=length(transmitted)/N;

for k=1:2*n-1 q=(k-1)*(N/2)+1; Xm(k,:)=transmitted(q:(q+N-1)); end
[M,N]=size(Xm); avgs=M; twin=hanning(N); gain = 0.5; BW = 1.5; twin=twin'/gain;
for k=1:M Xm(k,:)=Xm(k,:).*twin; end
Xm=fft(Xm)';
for k=1:M Xm(k,:)=Xm(k,:).*conj(Xm(k,:))/N^2; end
Xm=Xm(:,1:(N/2+1));
for k=1:M Xm(k,2:N/2)=2*Xm(k,2:N/2); end
if M ~ 1 Pxx=mean(Xm); else Pxx=Xm; end
deltaf=samplerate/N; freq=linspace(0,N/2,N/2+1)*deltaf;

transmitted=k*(displacement-y)+(c+cmr).*(velocity-ydot)+fyield;

% Fluid Properties Plot
figure(2)
subplot(3,1,1), plot(srf,visc,'k'), axis([0 150 -1 5])
title('MR Fluid Characteristics - MRF 132LD - Lord Corporation'), xlabel('Shear Rate (1/s)'),
ylabel('Viscosity (Pas)')
subplot(3,1,2), plot(Hf,ysf,'k'), axis([0 300000 0 50000])
xlabel('H (Amp/m)'), ylabel('Yield Stress (Pa)')
subplot(3,1,3), plot(Hf,Bf,'k'), axis([0 300000 0 1])
xlabel('H (Amp/m)'), ylabel('B (Tesla)')

% Absolute Amplitudes Plot
figure(3)
subplot(4,1,1), plot(t,y), ylabel('ROAD'), title('Absolute Amplitudes')
subplot(4,1,2), plot(t,displacement), ylabel('DISPLACEMENT (m)')
subplot(4,1,3), plot(t,velocity), ylabel('VELOCITY (m/s)')
subplot(4,1,4), plot(t,acceleration), ylabel('ACCELERATION (m/s^2)'), xlabel('Time (s)')

% Relative Amplitudes Plot
figure(4)
subplot(2,1,1), plot(t,reldispl), ylabel('R. DISPLACEMENT (m)'), title('Relative Amplitudes')
subplot(2,1,2), plot(t,relvel), ylabel('R. VELOCITY (m/s)')

% Isolation Forces
figure(5)
subplot(4,1,1), plot(t,spring), ylabel('SPRING (N)'), title('Isolation Forces')
subplot(4,1,2), plot(t,damper), ylabel('DAMPER (N)')
subplot(4,1,3), plot(t,transmitted), ylabel('TRANSMITTED (N)'), axis([0 2 -20 20])
subplot(4,1,4), plot(t,mrforce), ylabel('MRFORCE (N)'), xlabel('Time (s)')

```

% Flow Properties

```
figure(6)
subplot(3,1,1), plot(t,sr), ylabel('SHEAR RATE (1/s)', title('Flow Properties'))
subplot(3,1,2), plot(t,Q), ylabel('Volumetric Flow (m^3/s)')
subplot(3,1,3), plot(t,viscosity), ylabel('Viscosity'), xlabel('Time (s)')
```

% Flow Determination (Laminar or Turbulent)

```
figure(7)
subplot(2,1,1), plot(t,Re), ylabel('Reynolds Number'), title('Flow Determination (Laminar or Turbulent)')
subplot(2,1,2), plot(t,T), ylabel('T (SS Book)')
```

% Bingham Plastic Properties

```
figure(8)
subplot(2,1,1), plot(t,fyield), ylabel('FYIELD (N)'), title('Bingham Plastic Properties')
subplot(2,1,2), plot(t,cmr), ylabel('PASSIVE MR DAMPING (N*s/m)')
```

% Electro Magnetic Fluid Properties

```
figure(9)
subplot(3,1,1), plot(t,ys), ylabel('YIELD STRESS (Pa)'), title('Electro Magnetic Fluid Properties')
subplot(3,1,2), plot(t,H), ylabel('H (Amp/m)')
subplot(3,1,3), plot(t,B), ylabel('B (Tesla)'), xlabel('Time (s)')
```

% Isolator Results

```
figure(10)
subplot(3,1,1), plot(t,relvel), ylabel('RELATIVE VELOCITY (m/s)'), title('Isolator Results')
subplot(3,1,2), plot(t,power), ylabel('POWER (W)'), xlabel('Time (s)')
subplot(3,1,3), semilogy(freq,Pxx), axis([0 512 10^-4 10]), ylabel('PS Of Transmitted Force')
```

% MR Comparison

```
figure(11)
subplot(4,1,1), plot(t,cmrforce), ylabel('PASSIVE MR FORCE (N)'), title('MR Comparison')
subplot(4,1,2), plot(t,mryieldforce), ylabel('ACTIVE MR FORCE (N)')
subplot(4,1,3), plot(t,mrforce), ylabel('TOTAL MR FORCE (N)')
subplot(4,1,4), plot(t,pressure), ylabel('DELTA P (Pa)'), xlabel('Time (s)')
```

% Model Inputs

```
figure(12)
subplot(2,1,1), plot(t,Fcomp), ylabel('Compressor Input (N)'), title('Model Inputs'), axis([0 2 -20 20])
subplot(2,1,2), plot(t,y), ylabel('Vehicle Body Motion (m)'), axis([0 2 -.05 .05]), xlabel('Time (s)')
```

% Phase Comparison

```
figure(13)
```

```
plot(t,damper,'r',t,mryieldforce,'b'), legend('passive','active'), axis([0.9 1.3 -25 25])
title('Without Skyhook, active reacts at the same time as the passive.'), xlabel('Time (s)'),
ylabel('Damping Force (N)')
```

```
maxreldispl=max(reldispl) % Display Maximum Relative Displacement
maxpower=max(power) % Display Maximum Power Required
roadtrans=Pxx(6) % Display Road Input Portion Of The Power Spectrum Of The
Transmitted Noise
comptrans=Pxx(51) % Display Compressor Portion Of The Power Spectrum Of The Transmitted
Noise
```

APPENDIX D

- Coil design equations

Parameters To Determine Coil Volume

- Coil Inner Diameter
- Coil Maximum Outer Diameter
- Coil Width
-

Parameters Determined By Wire Gage

- Copper Diameter
- Insulation Thickness
- $InsulatedDiameter = CopperDiameter + 2(InsulationThickness)$

Determining Number Of Turns

$$\frac{\#turns}{layer} = \frac{CoilWidth}{InsulatedDiameter}$$
$$\#layers = \frac{(CoilID - CoilOD)}{2(InsulatedDiameter)(PackingHeight)}$$
$$\#turns = INT\left(\frac{\#turns}{layer}\right)INT(\#layers)$$

Coil Physical Properties

$$CoilActualOD = CoilID + (InsulatedDiameter)(PackingHeight)(INT(\#layers))$$
$$CoilAverageDiameter = \frac{CoilID + CoilActualOD}{2}$$
$$CoilLength = \pi(CoilAverageDiameter)(\#turns)$$
$$CoilMass = CoilLength \frac{CoilMass}{CoilLength}$$

Coil Electrical Properties

$$CoilResistance(@^{\circ}C) = CoilLength \frac{CoilResistance(@^{\circ}C)}{CoilLength}$$
$$Current = \frac{Voltage}{Resistance}$$
$$AmpTurns = (\#turns)(Current)$$

APPENDIX E

- Algorithm for compressor input
- Algorithm for vehicle body input
- Algorithm for lowpass filter
- Algorithm for skyhook control
- Algorithm for relative skyhook control

Compressor Variables

```
freqc=50; b=10; m=1; % Speed, amplitude of force, compressor mass
Fcomp(1:points)=0; % Forcing function of the compressor
Fcomp(1000:2750)=b*sin(2*pi*freqc*t(1:1751));
```

Vehicle Body Variables

```
% Vehicle Body Variables
freq1=1; omega1=2*pi*freq1; a=.00508; % Frequency and amplitude of body
freq2=5; omega2=2*pi*freq2; aa=.01905; % Frequency and amplitude of bump
y=a*sin(omega1*t); % Road displacement
y(4073:4472)=a*sin(omega1*t(4073:4472))% as a function of time
+aa*sin(omega2*t(1:400));
ydot=a*omega1*cos(omega1*t); % Road velocity
ydot(4073:4472)=a*omega1*cos(omega1*t(4073:4472)) % as a function
+aa*omega2*cos(omega2*t(1:400)); % of time
```

Low Pass Filter

```
v(i)=relvel(i); % Active Variable
if i>=3 % Lowpass Filter
    z(i)=C(1)*v(i)+C(2)*v(i-1)+C(3)*v(i-2)-A(2)*z(i-1)-A(3)*z(i-2);
elseif i==2
    z(i)=C(1)*v(i)+C(2)*v(i-1)+A(2)*z(i-1);
else
    z(i)=C(1)*v(i);
end
scale=25000; % Scale Factor For Yield Stress
ys(i)=z(i)*scale;
```

Skyhook Control

```
if vel*(vel-ydot(i))>0 %
    w(i)=relvel(i) % Skyhook
else % Control
    w(i)=0; %
end%
```

Relative Skyhook Control

```
if (vel-ydot(i))*(vel-ydot(i))>0 %
    w(i)=relvel(i) % Relative
else % Skyhook
    w(i)=0; % Control
end%
```